nature communications

Article

https://doi.org/10.1038/s41467-025-63110-0

Restoring mucosal barrier homeostasis by in situ formation of a living-synthetic therapeutic coating

Received: 8 December 2024

Accepted: 8 August 2025

Published online: 18 August 2025

Check for updates

Wei Yu[1,4], Huilong Luo[2,4], Bo Han[1], Sisi Lin[2], Qian Li[3], Rui Xue[1], Hui Tang[1], Xin Jia[1] ✉, Lu Wang[2] ✉ & Jinyao Liu[2] ✉

The mucosal barrier consisting of physicochemical, immune, and microbial components is the first line of defense against external stimuli. Breakdown of the mucosal barrier causes the occurrences of various diseases, while methods capable of multifacetedly restoring mucosal barrier functions have been rarely reported. Here, we describe the restoration of the physicochemical, immune, and microbial homeostasis of the mucosal barrier by in situ formation of a living-synthetic therapeutic coating (LSTC). Through metal-phenolic complexation and π-π stacking interactions, ethyl gallate can chelate Bi^{III} ions to form an adhesive coating on mucosal surfaces, which enables further hybridization with living bacteria. Due to the beneficial effects of Bi^{III} and ethyl gallate and the probiotic characteristic of carried bacteria, LSTC increases the barrier integrity, mitigates mucosal inflammation, and maintains normal homoeostasis of the microbiota. In two murine models of aerobic vaginitis and vaginal candidiasis, LSTC demonstrates the potency to alleviate vaginal pathological injury and decrease vaginal inflammatory infiltration.

The mucosal barrier is the first line of defense against infection and environmental insults as most noxious stimuli enter the body at mucosal surfaces[1–3]. Mucosal barrier homeostasis is primarily maintained by the combined effects of commensal microbiota, the physicochemical barrier, and mucosal immune responses[4,5]. The breakdown of the mucosal barrier may lead to the pathogenesis and progression of a variety of diseases, including infection, allergy, and inflammation[6–8]. Restoration of mucosal barrier functions has emerged as a promising approach to protect the host from exogenous stimuli. For example, immunoregulatory agents, such as anti-tumor necrosis factor (TNF) antibody drugs, are currently prevailing treatments to revert the dysregulated mucosal barrier through blocking a specific inflammatory pathway[9,10]. While, inhibition of immune functions often results in an increased risk of severe or even life-threatening infections[11]. Furthermore, several small molecule kinase inhibitors have been exploited to directly promote mucosal healing by reinforcing barrier integrity or increasing epithelial regeneration[12]. Unfortunately, the promotion of mucosal healing may cause abnormal cell proliferation and thus induce oncogenic transformation[13]. More importantly, the unitary modality of these therapeutics inevitably suffers an inadequate efficacy, due primarily to the inability to synergistically improve the microbial, immune, and physicochemical dysfunctions. Therefore, exploration of methods capable of restoring mucosal barrier functions to resist exogenous damaging factors is of great significance in disease treatment.

Mucosal surfaces are characteristically colonized by a living and dynamic microbial ecosystem as the direct exposure to external environments[14,15]. The microbiota plays a fundamental role in regulating mucosal barrier functions by dialoguing with the epithelium and mucosal immune system[16]. For instance, mucus-dwelling bacteria can

[1]School of Chemistry and Chemical Engineering, School of Pharmacy, Key Laboratory of Xinjiang Phytomedicine Resource and Utilization, Shihezi University, Shihezi, Xinjiang, China. [2]Shanghai Key Laboratory for Nucleic Acid Chemistry and Nanomedicine, Institute of Molecular Medicine, Renji Hospital, School of Medicine, Shanghai Jiao Tong University, Shanghai, China. [3]Xinjiang Military Command General Hospital, Urumqi, Xinjiang, China. [4]These authors contributed equally: Wei Yu, Huilong Luo. ✉e-mail: jiaxin@shzu.edu.cn; biowl@sjtu.edu.cn; jyliu@sjtu.edu.cn

degrade mucin produced by specialized epithelial cells and secrete metabolites that in turn influence mucus production and epithelial integrity[17,18]. Meanwhile, certain bacteria affect the functions of both the innate and adaptive immune systems to maintain immune homeostasis, yet microbiota dysbiosis can trigger several immune disorders through the activity of macrophages, neutrophils, or T cells[19,20]. Nevertheless, the breakdown of the epithelial barrier leads to immediate leakage of bacteria and bacterial derivatives, which contribute to systemic deterioration and subsequently aggravate the local destruction of the mucosal barrier[21,22]. In addition, inflammatory environment is conducive to the blooms of certain opportunistic pathogens, which secrete specific toxins to kill beneficial bacteria and promote the necrosis of epithelial cells[23]. Given these close mutual interactions, we hence speculate that the restoration of a healthy microbial structure together with the mitigation of physicochemical and immune dysfunctions may provide an alternative to recover mucosal barrier homeostasis. However, to the best of our knowledge, methods capable to multifacetedly orchestrate mucosal barrier functions have been rarely reported.

Here, we report the use of in situ formation of a living-synthetic therapeutic coating (LSTC) to restore the physicochemical, immune, and microbial homeostasis of the mucosal barrier (Fig. 1). With the help of metal-phenolic complexation and π-π stacking interactions, an ethyl gallate-Bi^{III} coating hybridized with living bacteria can be readily generated on mucosal surfaces. We show that LSTC is flexible to hybridize diverse bacterial strains and can be steadily formed on the surface of different types of mucosae. By perfusing Bi^{III} ions, ethyl gallate (EG), and *Lactobacillus rhamnosus* GG (LGG), the resulting LSTC is able to restore the physicochemical, immune, and microbial functions of the mucosal barrier, thanks to the combination of the barrier-repairing ability of Bi^{III} ions, the immunosuppressive nature of EG, and the microbiota-regulating behavior of LGG. Consequently, LSTC recovers the barrier integrity by elevating the expressions of tight junctions and mucus, alleviates mucosal inflammation by suppressing inflammasome activation, and maintains normal homeostasis of the microbiota by inhibiting the colonization of pathogens.

Vagina is a major mucosal interface connecting the inner and outer environments in the body[24]. Vaginal infections, one of the most common reasons for women medical consultation, influence about 75% of adult women worldwide each year[25]. Although vaginal infections are not associated with high mortality rate, they severely increase the risk of serious consequences, including infertility, cervical cancer, and acquisition of the human immunodeficiency virus[26–28]. Currently available treatments are antimicrobial therapy, which is effective but has a high incidence of recurrence and potential risk of causing antibiotic resistance[29,30]. As a proof-of-concept application, we show that

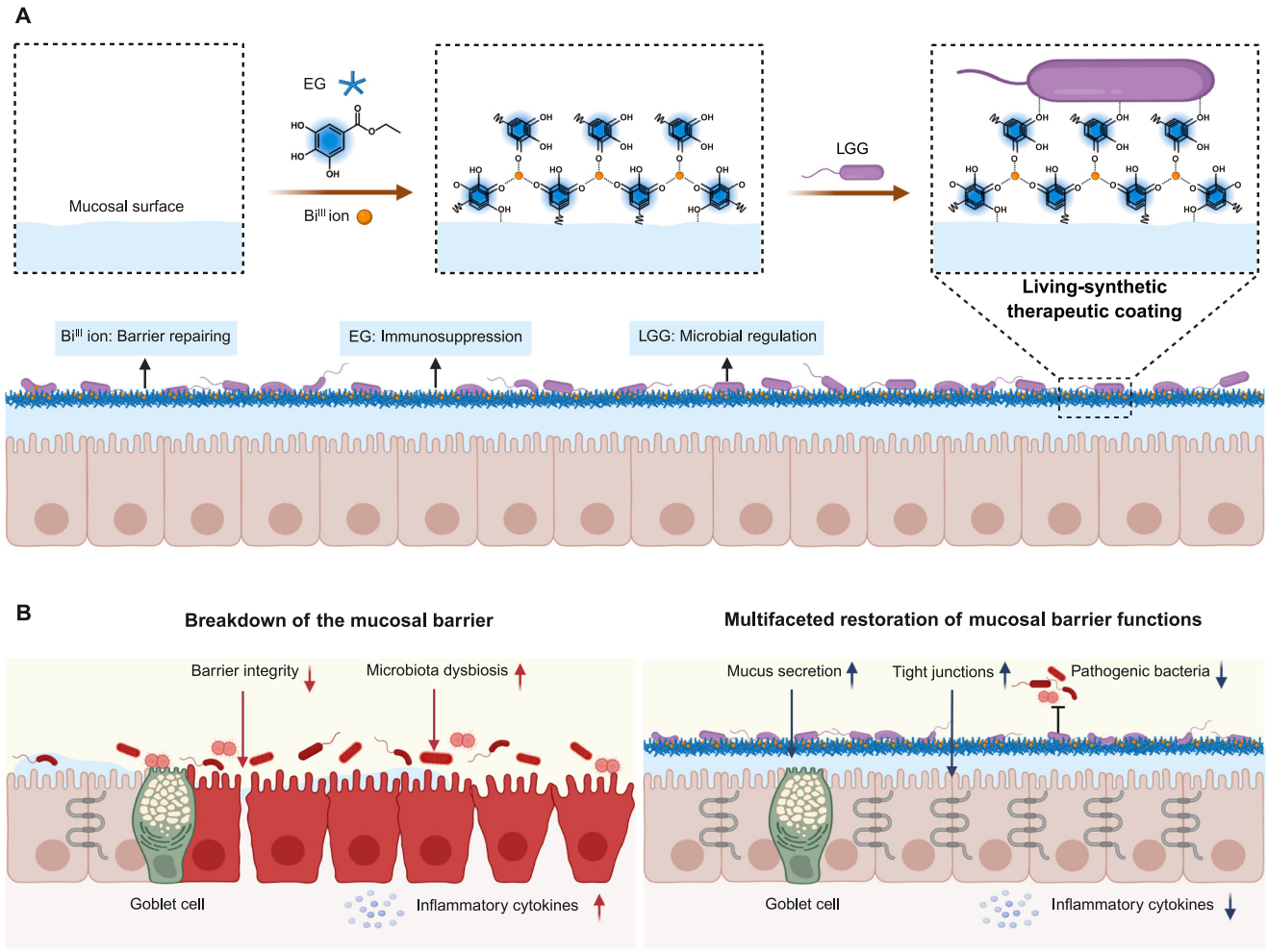

Fig. 1 | Schematic illustration. A Preparation of LSTC by in situ forming an EG-Bi^{III} coating hybridized with living LGG on the mucosal surface. **B** Combination of the barrier-repairing ability of Bi^{III} ions, the immunosuppressive feature of EG, and the microbiota-regulating behavior of LGG enables LSTC to multifacetedly restore mucosal barrier functions. Specifically, LSTC improves barrier integrity by increasing the secretions of tight junctions and mucus, remits mucosal inflammation by suppressing the production of inflammatory cytokines, and maintains normal homeostasis of the microbiota by inhibiting the colonization of pathogens. Created in BioRender.

following vaginal delivery, LSTC exhibits satisfactory efficacies in treating vaginal infections, supported by the potency to alleviate vaginal pathological injury and reduce vaginal inflammatory infiltration in two mouse models of aerobic vaginitis and vaginal candidiasis. We anticipate that LSTC provides a versatile platform to orchestrate multifaceted barrier functions via synergizing bacterial agents with conventional therapeutics at the interface of mucosae.

Results and discussion

Preparation and characterization of LSTC

Previously, metal-polyphenol complexes have been employed to coat bacteria and improve their intraluminal colonization for enhanced inflammation treatment[31]. While the therapeutic potential of metal-polyphenol complexes coated on bacterial surface is limited due to their overall low dose and negligible amount adhered to the mucosal surface. Therefore, we chose the formation of a metal-polyphenol coating hybridized with living bacteria on the mucosal surface to play a therapeutic effect. LGG, which has been chosen as a model probiotic, because it widely resides the mucosal surfaces of the gastrointestinal, respiratory, and vaginal tracts and plays a pivotal role in host health[32–34]. To form LSTC, EG extracted from Turkish galls and Bi^{III} ions were separately selected considering the ability to suppress inflammation[35,36] and the activity to promote mucosa repair[37,38]. Note that both EG and Bi^{III} ions have been approved by the Food and Drug Administration for use as a food additive and a nutritional supplement[31,38,39], respectively. Through the formation of metal-phenolic complexation and π-π stacking interactions, EG could chelate Bi^{III} ions to form an adhesive coating, which was able to hybridize with LGG. To optimize the formation of the coating, EG and $Bi(NO_3)_3{\cdot}5H_2O$ solutions with different concentrations were successively added to an agar plate and mildly stirred for deposition. As shown in Supplementary Fig. 1, under the conditions of 0.6 mg/ml EG and 0.2 mg/ml $Bi(NO_3)_3{\cdot}5H_2O$, the resulted coating (termed EG-Bi) showed the highest efficiency for LGG attachment, accompanied by undetectable adverse effects on bacterial viability (Supplementary Fig. 2). The cytocompatibility of EG-Bi was verified using a cell counting kit-8 (CCK-8) assay, which displayed a negligible cytotoxicity against both epithelial and macrophage cell lines even after incubation for 24 h (Supplementary Fig. 3). We reasoned that the high cytocompatibility of EG-Bi could be attributed to relatively low dosage of EG and Bi^{III} ions used for preparation and rapid chelation during the coating process. Surface morphology of EG-Bi was characterized by scanning electron microscopy (SEM) and transmission electron microscopy (TEM), both suggesting a dense nanoparticulate surface structure (Fig. 2A, B). Atomic force microscopy (AFM) imaging further confirmed the formation of EG-Bi and highlighted that the thickness of the coating was 96.8 ± 1.1 nm (Fig. 2C). The water contact angle of silicon wafer surface decreased from 88.5 ± 2.0° to 13.9 ± 1.2° after decorating with EG-Bi (Fig. 2D), suggesting the hydrophilic surface property of the coating. As the mucosal barrier is generally covered with a gel-forming mucus layer[40], the plate surface was coated with an artificial mucus layer containing commercial mucin and agar to assess whether EG-Bi could form on such a surface. In contrast, obviously increased fluorescence signaling in the FITC channel was observed in the EG-Bi group after staining the surface with fluorescein isothiocyanate-labeled bovine serum albumin (BSA-FITC) (Fig. 2E), verifying the decoration of EG-Bi on the mucus surface. We next evaluated the flexibility of EG-Bi and found that its thickness increased with the concentrations of EG and $Bi(NO_3)_3{\cdot}5H_2O$. When the concentrations of EG and $Bi(NO_3)_3{\cdot}5H_2O$ were separately increased to 1.2 and 0.4 mg/ml, three-dimensional laser scanning confocal microscopy (3D LSCM) images showed a 1.5-fold increment in EG-Bi thickness (Fig. 2F).

Next, we studied the formation of LSTC by examining the hybridization of living bacteria onto EG-Bi. After incubation EG-Bi with LGG for 5 min, SEM and TEM images visualized the increased amounts of LGG on the EG-Bi surface compared to those of undecorated mucus surface (Fig. 2G and Supplementary Fig. 4). Leveraging Cy5.5-labeled LGG to form LSTC, the anchored bacteria were visually confirmed by LSCM, which displayed an obvious fluorescence signaling in the EG-Bi group (Fig. 2H). To quantify the number of hybridized bacteria, 5.0×10^7 colony-forming units (CFUs) of LGG was added onto the area of 4.5 cm^2 of EG-Bi for 24-h incubation. The anchored LGG were collected for bacterial plate counting, verifying that LGG exhibited a 9.8-fold increase on the EG-Bi surface compared to the undecorated one (Fig. 2I). In addition, we calculated that about 2.7×10^7 CFUs of LGG could be attached to the area of 4.5 cm^2 of EG-Bi. We then explored the versatility of EG-Bi to bind diverse probiotic strains, including Gram-positive *Enterococcus faecalis* (EF) and *Lactobacillus delbrueckii* subsp. *bulgaricus* (LD) as well as Gram-negative *Escherichia coli* Nissle 1917 (EcN). Similar to that of LGG, an increased amount of EF, LD, or EcN was also visualized on the EG-Bi surface (Fig. 2G, H, and Supplementary Fig. 4). In comparison to that of naked mucus surface, bacterial plate counting showed a 20.7-, 30.1-, and 37.2-fold higher attachment of EF, LD, and EcN on the EG-Bi surface, respectively (Fig. 2I). Taken together, these results verified that LSTC could be implemented readily to mucus surface in vitro.

Formation of LSTC on mucosal surfaces

Having confirmed the successful preparation of LSTC in vitro, we then attempted to perform LSTC on mucosal surfaces. First, the validity of the formation of LSTC at different mucosal interfaces was assessed using ex vivo models. Cy5.5-labeled LGGs were used to form LSTC, which was subsequently imaged using in vivo imaging system (IVIS). Vaginal mucosal interface is unique because it must adapt to complicated physiological situations, such as acidic pH and hormonal fluctuation[41]. As such, the vaginal tract was sampled from mice and exposed to the LSTC solution containing 0.6 mg/ml EG, 0.2 mg/ml $Bi(NO_3)_3{\cdot}5H_2O$, and 1.0×10^6 CFUs/ml Cy5.5-labeled LGG (termed EG-Bi-LGG). Equivalent Cy5.5-labeled LGG were set as a control. Clearly, IVIS images presented a higher fluorescence intensity in the vaginal tissues after decorating with LSTC (Fig. 3A, B), suggesting the feasibility to form LSTC at the mucosal interface within the vaginal tract. To quantify the number of introduced bacteria in LSTC, vaginal tissues were homogenized for bacterial plate counting. In contrast to the control group, EG-Bi-LGG presented a 5.9-fold increment in the adhesion of LGG to the vagina lining (Fig. 3C). In addition, we measured the concentration of Bi^{III} ions in the decorated tissues by inductively coupled plasma mass spectrometry (ICP-MS). As plotted in Fig. 3D, the content of Bi^{III} ions in the EG-Bi-LGG group was substantially higher than that in the control group, further demonstrating the presence of Bi^{III} ions in the coating. The gastrointestinal tract is the most widely studied among all mucosal tissues[42]. In agreement with the results from the vaginal tract, LSTC could efficiently form on the mucosal surface of the intestinal tract, reflected by a clearly stronger fluorescence signal and a 4.9-fold increase in bacterial number in the decorated colonic tissues (Fig. 3E–G).

We further evaluated whether LSTC could be conducted in vivo. Mice were intravaginally dosed by a two-step procedure and equivalent Cy5.5-labeled LGG was applied as a control. It was worth mentioning that the mixing of EG and Bi^{III} ions as well as the injection, was conducted rapidly to avoid the formation of a massive complex structure (Supplementary Fig. 5). At 6 h after administration, IVIS images of mice treated with EG-Bi-LGG exhibited noticeably enhanced fluorescence intensity in the vagina, which was further confirmed by ex vivo imaging of the collected vaginal tract (Fig. 3H, I). As given in Fig. 3J, quantification of LGG attached to the vaginal tract exhibited a 4.5-fold increase in the EG-Bi-LGG group. The above data validated in vivo formation of LSTC at the vagina. Moreover, rectal administration of the LSTC solution to mice enabled elevated fluorescence intensity and enriched bacterial distribution in the sampled colonic

https://doi.org/10.1038/s41467-025-63110-0

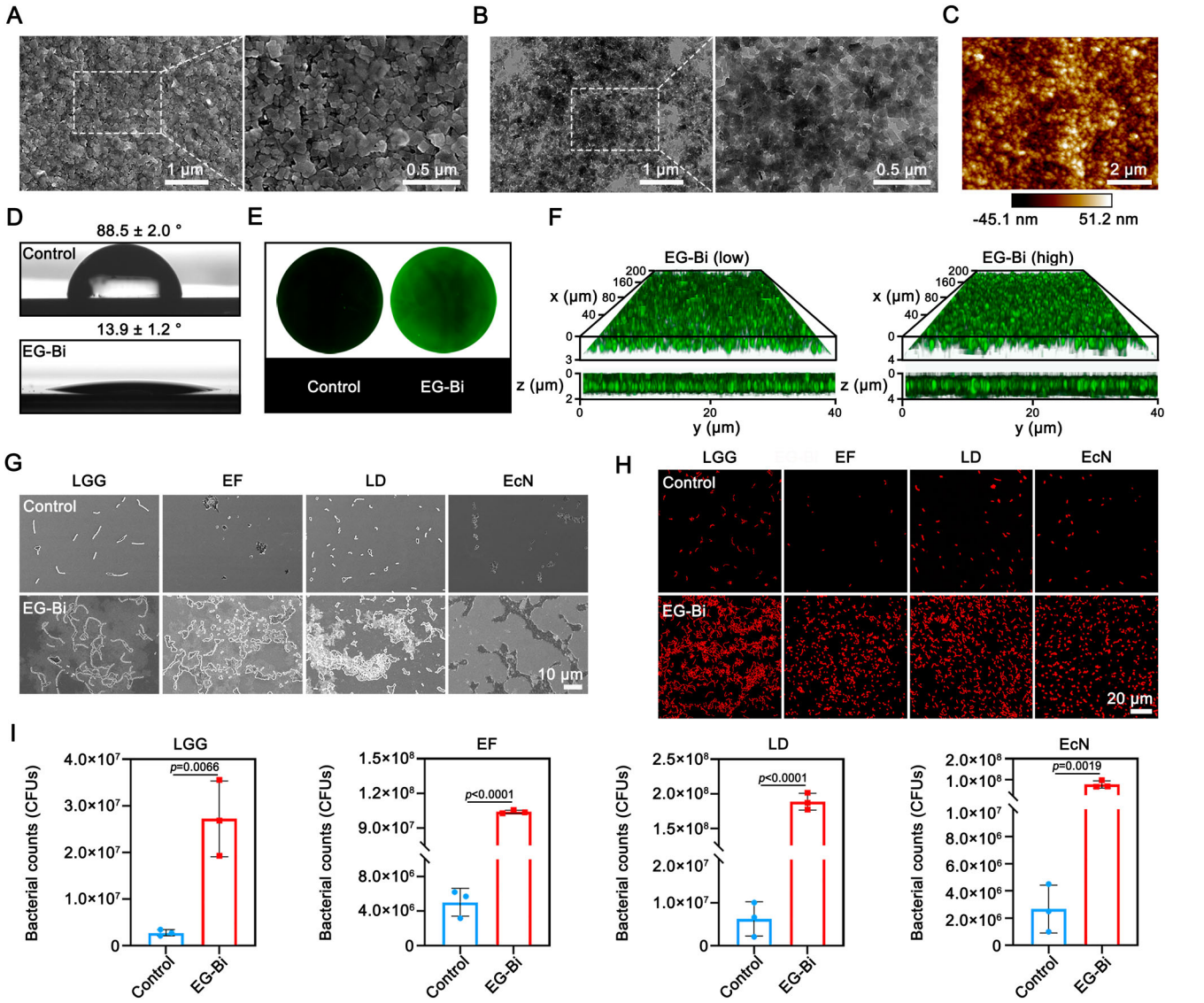

Fig. 2 | Characterization of LSTC. SEM (**A**), TEM (**B**), and AFM (**C**) images of the EG-Bi coating. The experiment was independently repeated at least twice with similar results. **D** Water contact angles of the EG-Bi coating tableted on silicon wafer. **E** Fluorescence images of the EG-Bi coating labeled with BSA-FITC. **F** 3D LSCM images of the EG-Bi coating with a relatively low (0.6 mg/ml EG and 0.2 mg/ml $Bi(NO_3)_3{\cdot}5H_2O$) or high (1.2 mg/ml EG and 0.4 mg/ml $Bi(NO_3)_3{\cdot}5H_2O$) concentration. SEM (**G**) and LSCM (**H**) images of LSTC containing LGG, EF, LD, or EcN. Red channels indicate Cy5.5-labeled or mCherry-expressing bacteria. **I** Counts of adherent LGG, EF, LD, or EcN on LSTC after a 24-h culture on MRS or LB agar plates at 37 °C ($n = 3$ independent samples). LSTC without the EG-Bi coating was used as a control in **D**, **E**, **G**, **H**, and **I**. Data are mean ± standard deviation (SD). Statistical analysis was performed using a two-tailed Student's *t*-test, and *p*-values were indicated. Source data are provided as a Source Data file.

tissues of the EG-Bi-LGG group, thoroughly verifying the formation of LSTC on the inner lining of the intestine (Fig. 3K–M). To investigate the duration of LSTC, mice vaginally administered with the LSTC solution were monitored using IVIS at a 6-h interval for 2 days. We found that treatment with LGG alone emerged a rapid attenuation of fluorescence signal at the vagina within 12 h (Fig. 3N, O). In contrast, the EG-Bi-LGG group remained a higher degree of fluorescence signal than the LGG group even 2 days post-administration. The quantification of adherent LGG in the vagina confirmed that the amount of LGG in the EG-Bi-LGG group was significantly higher in comparison to that of the control group at least within 24 h (Supplementary Fig. 6A). The stability of LSTC was further interrogated by evaluating the retention of Bi^{III} ions in the vaginal tract. As shown in Supplementary Fig. 6B, the content of Bi^{III} ions in the vaginal mucosa of the EG-Bi-LGG group exhibited a gradual decline over time, yet remained at a higher level than the control group 24 h after administration. Collectively, these data validated the formation of LSTC on the surface of different types of mucosae in vivo.

Restoration of the mucosal physicochemical barrier by LSTC

Encouraged by the establishment of LSTC on mucosal surfaces, we then turned our attention to evaluating the influence of LSTC on the physicochemical barrier of the mucosa. Tight junctions, such as occludin and zonula occludens-1 (ZO-1), are intercellular adhesion complexes in epithelia and play a critical role in maintaining the integrity of the mucosal physicochemical barrier[43,44]. Given the fact that Bi-containing compounds have a protective effect on gastric mucosa[37,38,45], we ascertained the impact of $Bi(NO_3)_3{\cdot}5H_2O$ on the expression of tight junctions. As plotted in Supplementary Figs. 7, 8, stimulation with lipopolysaccharide (LPS) dramatically destroyed the tight junctions on the surface of both Caco-2 intestinal and VK2 vaginal

https://doi.org/10.1038/s41467-025-63110-0

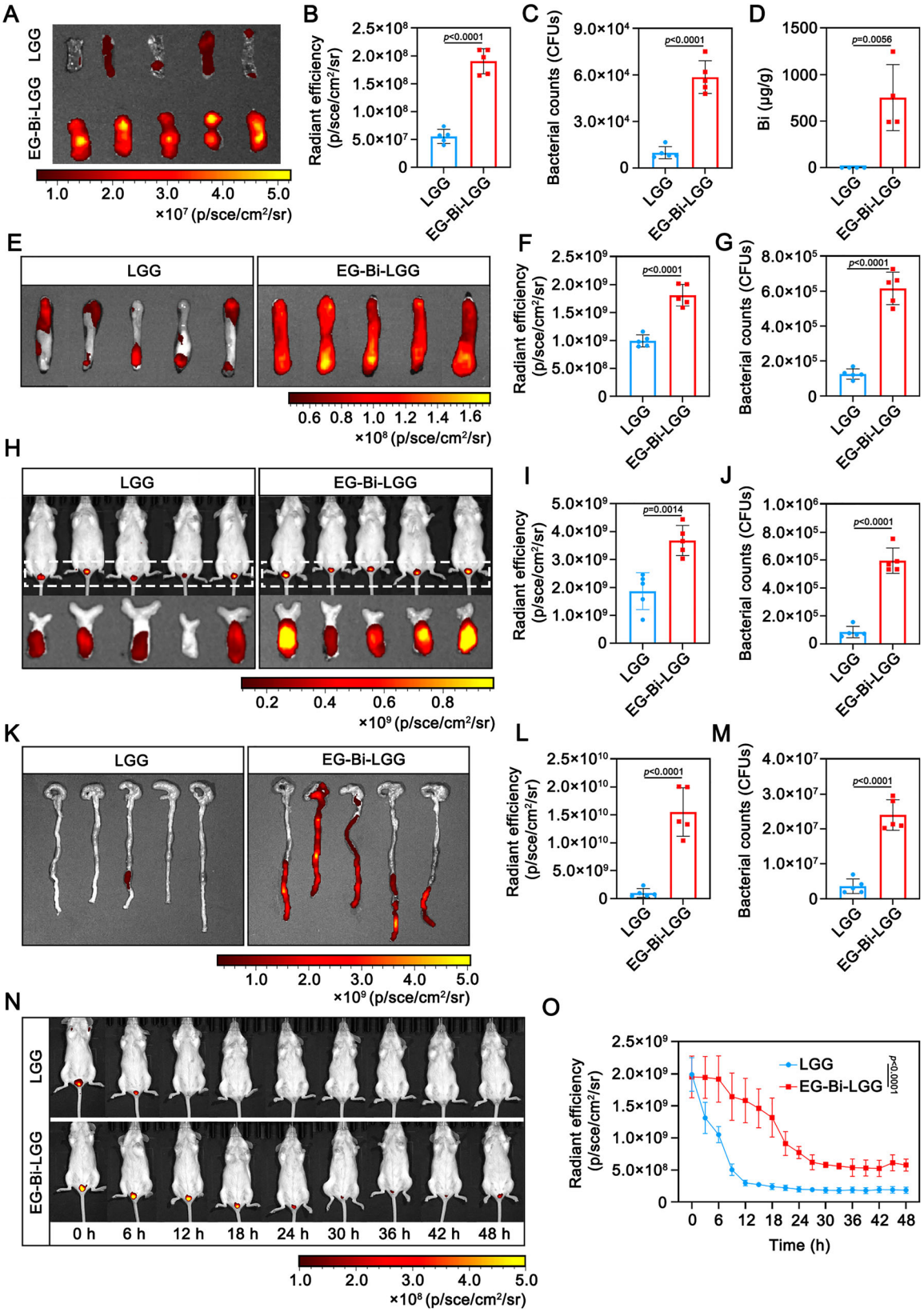

epithelial cells, as reflected by the decreased levels of occludin and ZO-1. Incubation with $Bi(NO_3)_3{\cdot}5H_2O$ significantly enhanced the expressions of occludin and ZO-1, suggesting the ability of Bi^{III} ions to recover the physicochemical barrier of the mucosa. Goblet cells are specialized epithelial cells responsible for the secretion of mucus, which in turn coats the intestinal epithelia to play a key role in mucosal physicochemical barrier[46,47]. On the basis of this notion, LPS-stimulated HT29-MTX-E12 goblet cells were co-cultured with $Bi(NO_3)_3{\cdot}5H_2O$ to assess mucus secretion. Images of alcian blue (AB) staining showed an immense decrease in mucus production after LPS stimulation, which was reversed by treatment with $Bi(NO_3)_3{\cdot}5H_2O$ (Fig. 4A). The data validated that Bi^{III} ions were able to effectively repair the destroyed

Fig. 3 | Formation of LSTC on diverse mucosal surfaces. IVIS image (**A**) and corresponding quantification of fluorescence intensity (**B**) of vaginal tissue after incubation with LGG or LSTC solution ($n = 5$ independent samples). **C** Counts of adherent LGG on vaginal surface after a 24-h culture on MRS agar plates at 37 °C ($n = 5$ independent samples). **D** Content of Bi^{III} ions on vaginal surface detected by ICP-MS ($n = 4$ independent samples). IVIS images (**E**) and corresponding quantification of fluorescence intensity (**F**) of colonic segments with a length of ~1.5 cm after incubation with LGG or LSTC solution ($n = 5$ independent samples). **G** Counts of adherent LGG on colonic surface after a 24-h culture on MRS agar plates at 37 °C ($n = 5$ independent samples). **H** IVIS images of mice and the sampled vaginal tracts at 6 h after intravaginal administration with LGG or LSTC ($n = 5$ independent samples). **I** Fluorescence intensity derived from the IVIS images of mice ($n = 5$ independent samples). **J** Counts of LGG collected from the vaginal tracts ($n = 5$ independent samples). IVIS images of the sectioned colon 6 h post-administration (**K**) and corresponding quantification of fluorescence intensity ($n = 5$ independent samples) (**L**). **M** Counts of LGG collected from the sectioned colon ($n = 5$ independent samples). IVIS images (**N**) and corresponding quantification of fluorescence intensity (**O**) of mice at various time points after intravaginal administration with LGG or LSTC ($n = 5$ independent samples). Fluorescence signal indicates bacteria labeled with Cy5.5. Data are mean ± SD. Statistical analysis was performed using two-tailed Student's *t*-test (**B**, **C**, **D**, **F**, **G**, **I**, **J**, **L**, **M**) or two-way ANOVA with Fisher's LSD multiple comparisons test (**O**), and *p*-values were indicated. Source data are provided as a Source Data file.

physicochemical barrier of the mucosa. Furthermore, the barrier integrity was confirmed by measuring transepithelial electrical resistance (TEER) and transepithelial permeability. TEER measurement reflects the ionic conductance of the intercellular pathway by assessing the electrical resistance across a cellular monolayer[48]. VK2 cells were seeded to the transwell insert and cultured for 4 days to form an epithelial cell monolayer. In comparison to the unstimulated control, the LPS-stimulated monolayer displayed a significantly reduced TEER value (Fig. 4B), which was nearly increased to a normal level after incubation with $Bi(NO_3)_3{\cdot}5H_2O$. Transepithelial permeability was tested by adding fluorescein isothiocyanate (FITC)-dextran to the transwell insert. As shown in Fig. 4C, an enhanced fluorescence signal was presented in the basolateral medium after stimulation with LPS, implying an increase in permeability across the monolayer. Similarly, treatment with $Bi(NO_3)_3{\cdot}5H_2O$ effectively reversed the permeability of FITC-dextran to a level comparable to that of the unstimulated one.

To evaluate the efficacy of LSTC in recovering the physicochemical barrier in vivo, two mouse models of impaired mucosal barrier, separately induced by vaginal infection of bacteria and fungi, were developed. To establish an aerobic vaginitis model, mice were intraperitoneally treated with 0.2 mg of estradiol benzoate every day for 3 days and subsequently infected with 4.0×10^7 CFUs of *S. aureus* every day for 7 days. Mice were intravaginally treated with the LSTC solution every day for 7 days. Healthy mice and infected mice treated with phosphate-buffered saline (PBS), LGG, or equivalent EG-Bi were separately set as controls. Vaginal tissues were collected to evaluate mucosal barrier functions by assessing the production of mucus and tight junctions 7 days post treatment. Alexa Fluor 488-labeled wheat germ agglutinin (AF488-WGA) was used to specifically label mucin, the major structural component of mucus. Fluorescence images of vaginal tissues presented a dense mucus layer covering the vaginal epithelium of healthy mice (Fig. 4D, E). Obviously, a dramatic decrease in mucin was observed after *S. aureus* infection, confirming the impairment of the mucosal barrier. Although treatment with EG-Bi could elevate the mucin level, EG-Bi-LGG resulted in the highest mucin level among all the groups. In addition, *S. aureus* infection caused a significant reduction in the expressions of occludin and ZO-1 of vaginal epithelium, which were greatly restored by EG-Bi-LGG (Fig. 4F–H). In line with above data, the recovery of mucus and tight junction productions in vaginal epithelium by EG-Bi-LGG was also demonstrated in mice infected by *C. albicans* (Supplementary Figs. 9, 10). Note that mice treated with EG-Bi-LGG exhibited a comparable level of occludin to that of healthy mice, yet a significantly lowered expression of ZO-1 compared to healthy mice. We speculated that EG-Bi-LGG preferentially affected the expression of occludin, which extends into the intercellular spaces to regulate the barrier permeability[43]. Briefly, LSTC was able to effectively restore physicochemical barrier integrity, which was largely attributed to the protective effect of Bi^{III} ions.

Alleviation of mucosal inflammation by LSTC

Excessive inflammation at the mucosal interface can induce the necroptosis of epithelial cells, contributing to the breakdown of the mucosal barrier[49,50]. We next investigated whether LSTC could suppress mucosal inflammation to maintain the homeostasis of the immune barrier. As a natural polyphenol, EG possesses an anti-inflammatory property that inhibits inducible nitric oxide synthase (iNOS) expression in macrophages[36,51]. To assess the anti-inflammatory effect of EG, LPS-stimulated J774A.1 cells, a macrophage cell line, were co-cultured with different concentrations of EG. As shown in Fig. 5A–C, LPS stimulation significantly increased the production of pro-inflammatory cytokines, including interleukin-1β (IL-1β), IL-6, and TNF-α, compared to the unstimulated group. Treatment with EG greatly blunted the levels of pro-inflammatory cytokines, especially IL-1β and IL-6, in a dose-dependent manner. Meanwhile, LPS enhanced the levels of late apoptosis and necrosis of epithelial cells, which were obviously reversed by EG (Fig. 5D and Supplementary Fig. 11). These data prompted us to evaluate the in vivo efficacy of LSTC in suppressing inflammation. Mice intravaginally infected by *S. aureus* were administered with the LSTC solution every day for 7 days and subsequently vaginal tissues were collected for messenger RNA sequencing (mRNA-Seq). Differential expression gene (DEG) analysis suggested that there were 134 downregulated and 349 upregulated DEGs in the vaginal tissue of the infected group compared to those of the healthy group (Fig. 5E). Among the upregulated DEGs in the infected tissue, 15, 5, and 218 genes were significantly downregulated after separately treating with LGG, EG-Bi, and EG-Bi-LGG, displaying a superior ability of EG-Bi-LGG in alleviating *S. aureus*-induced inflammatory activation. Pathway analysis using Kyoto Encyclopedia of Genes and Genomes (KEGG) or Gene Ontology (GO) enrichment evidenced that in comparison to the infected mice, the downregulated genes in the EG-Bi-LGG group were enriched in immune-related pathways (Fig. 5F, G). Gene-set enrichment analysis (GSEA) further confirmed the downregulated immune-related pathways, including inflammatory response, cytokine-cytokine interaction, Toll-like receptor signaling pathway, antigen processing and presentation, natural killer cell mediated cytotoxicity, activation of immune response, lymphocyte mediated immunity, immunoglobulin mediated immune response, and B cell mediated immunity (Fig. 5H and Supplementary Fig. 12). Of note, EG-Bi-LGG contributed to the decreased expression of numerous genes related to inflammasome (Supplementary Fig. 13). Cell type enrichment analysis was also conducted to quantify immune cell distribution within the vagina. As descripted in Fig. 5I, S. *aureus* infection caused a significant enrichment of innate immune cells, including granulocyte-monocyte progenitors, neutrophils, macrophages, and myeloid dendritic cells. This observation was in line with the notion that granulocyte-monocyte progenitors are capable of differentiating into neutrophils, macrophages, or dendritic cells in response to infection, which is the major pathway to produce pro-inflammatory cytokines[52]. In contrast, treatment with EG-Bi-LGG profoundly decreased the level of these cells compared to EG-Bi and LGG. Additionally, we found that *S. aureus* infection elicited an obvious B cell-associated activation, yet inhibited the T cell immunity, including both $CD8^+$ T cells and T-helper 1 (Th1) cells. Intriguingly, treatment with EG-Bi-LGG preferred to boost the activation of $CD8^+$ T cells and Th1 cells, which are the major subsets to mediate effective anti-infection immunity[53,54]. These results elucidated that EG-Bi-LGG effectively

https://doi.org/10.1038/s41467-025-63110-0

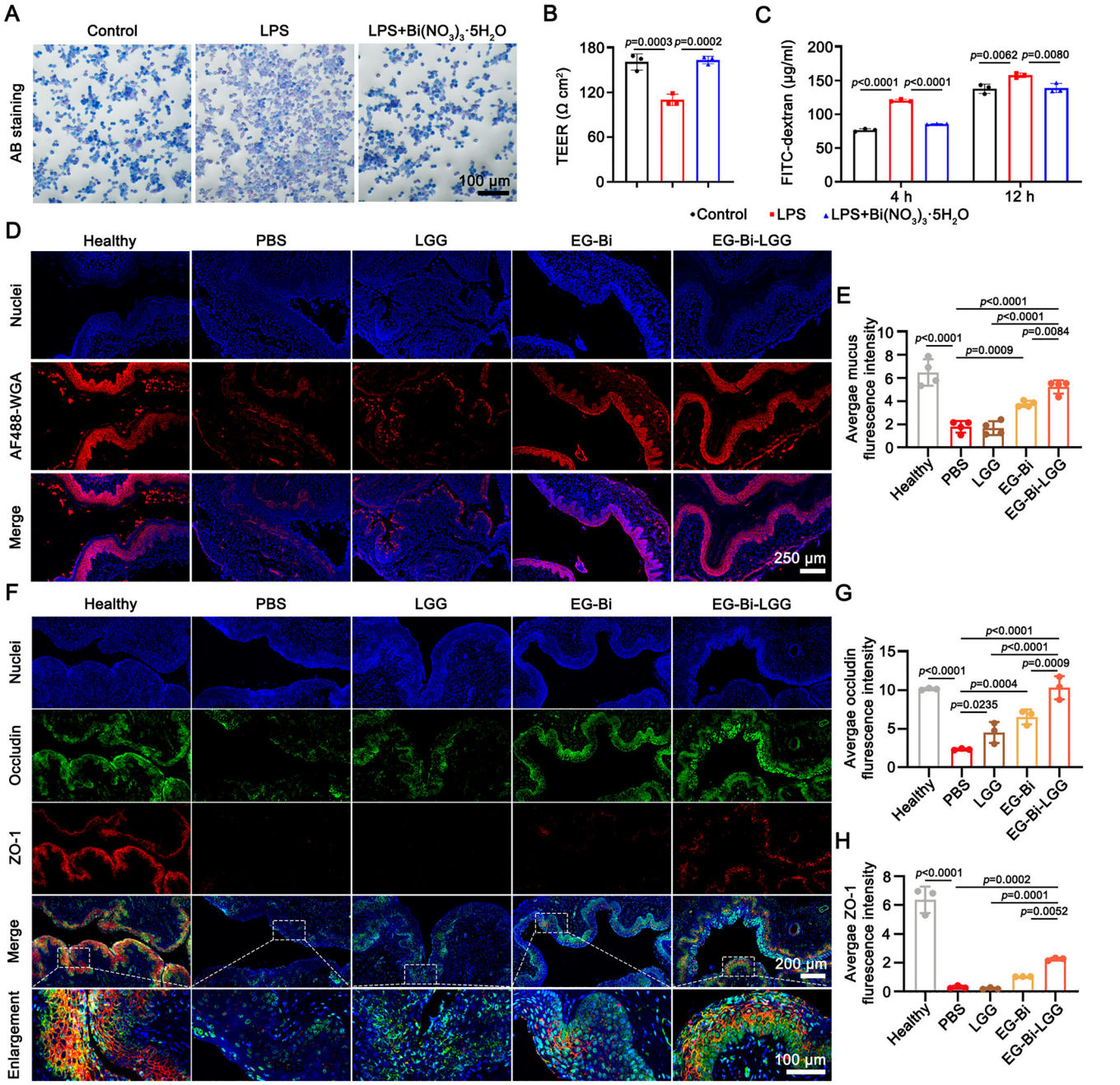

Fig. 4 | Restoration of the mucosal physicochemical barrier. A Images of AB staining of LPS-stimulated HT29-MTX-E12 cells incubated with PBS or 0.2 mg/ml $Bi(NO_3)_3{\cdot}5H_2O$ for 12 h. **B** TEER data of LPS-stimulated epithelial cell monolayer in transwell insert after incubation with PBS or 3 μg/ml $Bi(NO_3)_3{\cdot}5H_2O$ for 24 h ($n = 3$ independent samples). **C** Concentrations of FITC-dextran in the basolateral medium of transwell measured by a microplate fluorometer after incubation with PBS or 3 μg/ml $Bi(NO_3)_3{\cdot}5H_2O$ for 4 or 12 h ($n = 3$ independent samples). Control group indicates unstimulated cells in (**A**–**C**). **D**-**H** Evaluation of vaginal barrier integrity of *S. aureus*-infected mice after intravaginal treatment with PBS, LGG, EG-Bi, or EG-Bi-LGG every day for 7 days. **D** Images of AF488-WGA (red) staining of vaginal sections from treated mice. Blue indicates cell nuclei stained with 4′,6-diamidino-2-phenylindole (DAPI). **E** Average fluorescence intensity of AF488-WGA of vaginal sections from **D** ($n = 4$ independent samples). **F** Immunofluorescence images of vaginal occludin (green) and ZO-1 (red) expressions from treated mice. Blue indicates cell nuclei stained with DAPI. Average fluorescence intensities of occludin (**G**) and ZO-1 (**H**) of vaginal sections from (**F**) ($n = 3$ independent samples). Data are mean ± SD. Statistical analysis was performed using one-way ANOVA with Fisher's LSD multiple comparisons test, and *p*-values were indicated. Source data are provided as a Source Data file.

downregulated the inflammatory responses and triggered an anti-infection immunity within the vagina.

Regulation of the microbiota by LSTC

Next, the probiotic effect of LSTC on imbalanced microbial barrier of the mucosa was evaluated by assessing the homeostasis of the vaginal microbiota. Given that LGG has been reported to directly antagonize vaginal pathogen proliferation through peroxide or acid production[32,55], we tested the potency by co-culturing with *S. aureus* and *C. albicans*, respectively. As shown in Fig. 6A, LGG inhibited the growth of *S. aureus* in a dose-dependent manner. Particularly, LGG displayed a potent antagonistic effect on *C. albicans*, as reflected by substantially inhibited proliferation even with the feed ratio decreasing to 1:1 (Fig. 6B). In addition, we further tested the adhesion and

https://doi.org/10.1038/s41467-025-63110-0

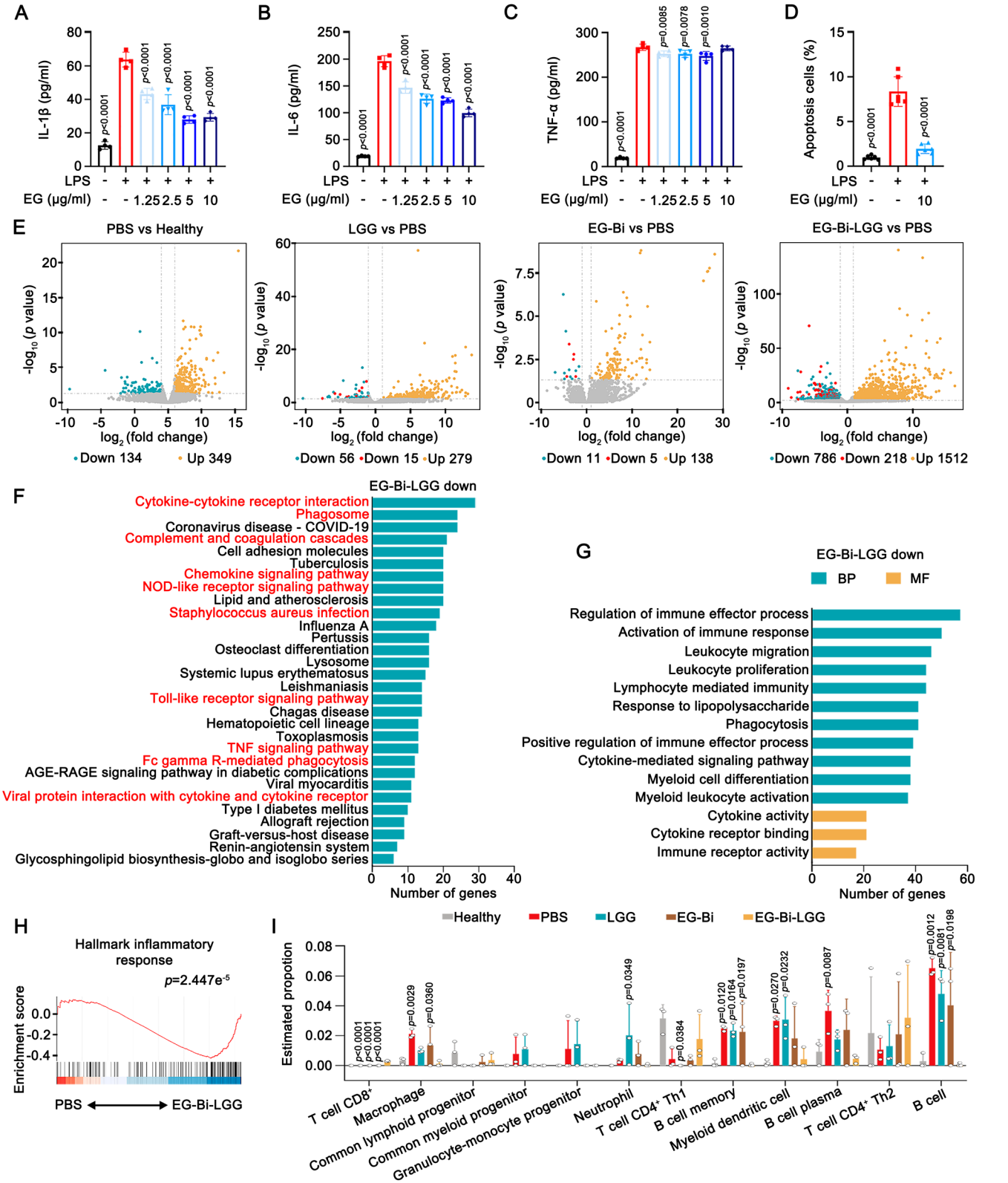

growth of vaginal pathogens on LSTC. In comparison to undecorated mucus surface, an increased amount of *S. aureus* or *C. albicans* on the LSTC surface was observed after a 4-h incubation (Supplementary Fig. 14A, B), suggesting the enhanced adhesion of vaginal pathogens to LSTC. Worth noting, monitoring the growth dynamics of *S. aureus* or *C. albicans* over a 24-hour period revealed that LSTC presented the most significant ability in inhibiting the growth of pathogens (Supplementary Fig. 14C, D). To ascertain the in vivo efficacy of LSTC in inhibiting pathogens and regulating the microbiota, mice were intravaginally infected with 4×10^7 CFUs of GFP-expressing *S. aureus*. After administration with the LSTC solution every day for 7 days, vaginal tissues were sampled to evaluate the counts of *S. aureus*. Healthy mice and infected mice treated with PBS, clindamycin, LGG, or equivalent EG-Bi were separately carried out as controls. Fluorescence images of the sampled vaginal tissues suggested that LGG treatment presented a reduction in *S. aureus* count compared to infected mice (Fig. 6C, D). Of

Fig. 5 | Alleviation of mucosal inflammation. Levels of IL-1β (**A**), IL-6 (**B**), and TNF-α (**C**) in the culture supernatant of LPS-stimulated J774A.1 cells incubated with different concentrations of EG ($n = 4$ independent samples). **D** Percentages of late apoptotic or necrotic VK-2 cells (Annexin V^+PI^+) stimulated with LPS after treatment with PBS or 10 μg/ml EG ($n = 6$ independent samples). Control group indicates unstimulated VK-2 cells. **E**–**I** *S. aureus*-infected mice were intravaginally administered with PBS, LGG, EG-Bi, or EG-Bi-LGG every day for 7 days and vaginal samples were collected for mRNA-Seq ($n = 3$). **E** Volcano plots showing differentially expressed genes in the PBS group compared to the healthy group and in the LGG, EG-Bi, or EG-Bi-LGG group compared to the PBS group, respectively. Red points indicate genes upregulated in the PBS group compared to the healthy group. vs, versus. **F** KEGG pathway enrichment analysis of the differentially expressed genes that were downregulated in the EG-Bi-LGG group compared to the PBS group ($p < 0.05$) and the top 30 enriched KEGG was shown. **G** GO enrichment analysis of the downregulated genes in the EG-Bi-LGG group from the PBS group ($p < 0.05$). BP and MF indicate biological process and molecular function, respectively. **H** GSEA showing enrichment of genes related to inflammatory responses. **I** Single-sample GSEA identifying the difference in immune infiltration in treated mice ($n = 3$ independent samples). Data are mean ± SD. p values in **A**–**D** indicate the statistical significance of various groups compared to the LPS-stimulated groups without EG treatment. p values in **I** indicate the statistical significance of various groups compared to the EG-Bi-LGG group. For **E**, DEGs were identified using DESeq2 ($|\log_2$ (fold change)$| \geq 1$ and FDR ≤ 0.05). For **F**, KEGG pathway enrichment was analyzed using a Fisher's exact test with Benjamini-Hochberg adjustment for multiple comparisons (adjusted p value ≤ 0.05). For **G**, GO enrichment was analyzed using a Fisher's exact test with Bonferroni, Holm, Sidak and FDR adjustment for multiple comparisons (adjusted p value ≤ 0.05). For **H**, GSEA was performed using R package clusterProfiler. Statistical analysis was performed using one-way ANOVA with Fisher's LSD multiple comparisons test (**A**–**D**, **I**), and p-values were indicated. Source data are provided as a Source Data file.

note, among all the treated groups, the most significant decrease of *S. aureus* was observed in the EG-Bi-LGG group. The microbial composition was analyzed using 16S ribosomal RNA gene sequencing. As expected, infected mice showed profoundly decreased richness of the vaginal microbiota, as reflected by a lower abundance-based coverage estimator (ACE) index and Chao1 index compared to healthy mice (Fig. 6E, F). In comparison to clindamycin, LGG, and EG-Bi, EG-Bi-LGG significantly augmented the richness of the vaginal microbiota. In addition, principal coordinates analysis (PCoA) at operational taxonomic unit (OTU) and genus levels indicated that infected mice presented an obvious difference in bacterial composition compared to healthy mice (Fig. 6G). In contrast to EG-Bi and clindamycin, treatments with LGG and EG-Bi-LGG displayed a similar bacterial composition to healthy mice, suggesting the reduced perturbation of the vaginal microbiota induced by *S. aureus* infection. Analysis of the relative abundance of bacteria at class level indicated that the microbial structure of mice treated with LGG or EG-Bi-LGG was closer to that of healthy mice (Fig. 6H). Specifically, EG-Bi-LGG increased the relative abundances of several probiotic bacterial genera, such as *Lachnospiraceae*_NK4A136 group and *Clostridium sensu stricto 1* (Fig. 6I, J). Worth noting, LSTC showed a superior ability to increase the richness and diversity of the vaginal microbiota compared to clindamycin, further demonstrating its potential to restore the homeostasis of the vaginal microbiota via restraining the expansion of pathogens and increasing the richness of probiotic bacterial genera.

Efficacy of LSTC in intervening aerobic vaginitis

Aerobic vaginitis is a common vaginal infection defined by a disruption in dominant *Lactobacillus* and an increase in aerobic enteric commensals or pathogens[56,57]. Different from other forms of vaginal infections, aerobic vaginitis presents more extreme inflammation and epithelial disruption[58]. In light of the effectiveness of LSTC in restoring mucosal barrier functions, we next evaluated its benefits in treatment of aerobic vaginitis (Fig. 7A). Mice were subcutaneously treated with estradiol benzoate every day for 3 days, followed by intravaginal infection with 10 μl of 4×10^9 CFUs/ml *S. aureus* every day for 7 days. To examine the therapeutic value of LSTC, infected mice were intravaginally administered with the LSTC solution every day for 7 days. Healthy mice and infected mice treated with PBS, LGG, or equivalent EG-Bi were separately carried out as controls. Clindamycin, a clinically used gold standard for aerobic vaginitis, was applied as a benchmark[59]. As shown in Fig. 7B, S. *aureus* infection caused a pronounced loss of body weight, which could be significantly recovered by clindamycin and EG-Bi-LGG. Vaginal washes were collected to quantify the number of *S. aureus* on day 8 after treatment, demonstrating that treatment with clindamycin and EG-Bi-LGG showed the most significant reduction in *S. aureus* number among all the treated groups (Fig. 7C, D). After infection, the vagina appeared red and swollen, which were substantially relieved after treatment with EG-Bi-LGG (Supplementary Fig. 15). Vaginal tissues of the treated mice were sampled to assess pathological injury using haematoxylin and eosin (H&E) staining. Compared to the healthy group, infected mice presented severe leukocyte infiltration and epithelial desquamation or keratinization (Fig. 7E). In contrast, the EG-Bi-LGG group exhibited a thinner and denser mucosal multilayer and a fewer leukocyte infiltration than infected mice with other treatments, implying an alleviated pathological injury of vaginal mucosal tissue. In addition, the levels of inflammatory cytokines, including IL-6, TNF-α, and IL-1β, in serum from EG-Bi-LGG-treated mice were reduced apparently in contrast to those of the PBS, LGG, and EG-Bi controls (Supplementary Fig. 16). Meanwhile, neutrophil infiltration of vaginal tissue was identified by myeloperoxidase (MPO), an enzyme mainly expressed in neutrophils. As depicted in Fig. 7F and Supplementary Fig. 17, MPO staining of the sectioned vaginal tissue indicated that treatment with EG-Bi-LGG greatly reduced the infiltration of MPO-positive cells compared to those of all other control groups. Besides, no pathological abnormality was observed after treatment in major organs, including the heart, liver, spleen, lung, and kidney, demonstrating satisfactory biosafety of LSTC (Supplementary Fig. 18). Together, LSTC verified its potency to alleviate aerobic vaginitis-associated pathological injury and inflammatory infiltration.

Potential of LSTC in treating vaginal candidiasis

Vaginal candidiasis commonly caused by *C. albicans* is one of the most prevalent fungal infections in the vagina[60]. Approximately 75% of women will be infected at least once in their lifetime, with about 8% suffering recurrent episodes[25]. Considering that *C. albicans* can grow in yeast, pseudohyphal, and hyphal morphologies, vaginal candidiasis exhibits a greater resistance to pharmacological treatments than aerobic vaginitis[32]. Next, we investigated the potential of LSTC in treating fungal infections by establishing a model of vaginal candidiasis (Fig. 8A). After subcutaneous injection of 0.2 mg estradiol benzoate every other day for three times, 2.0×10^7 CFUs of *C. albicans* were daily dosed into the vagina for 3 days. To assess the therapeutic effect of LSTC, infected mice were daily treated with the LSTC solution for 7 days. Healthy mice and infected mice treated with PBS, LGG, and equivalent EG-Bi were separately used as controls. Mice treated with 0.4 mg/kg of clinically used clotrimazole were used as a benchmark[61]. As evidenced in Fig. 8B, treatment with PBS, LGG, or EG-Bi had a negligible effect on the recovery of the decreased body weight caused by *C. albicans* infection. In contrast, EG-Bi-LGG presented an obvious benefit, implying its superior therapeutic efficacy. In comparison to PBS, LGG, or EG-Bi group, Periodic acid-Schiff (PAS) staining of vaginal secretions suggested a distinct decrease in fungal burden in mice treated with EG-Bi-LGG (Fig. 8C), which was in accordance with the relief of red and swollen vaginal appearance (Supplementary Fig. 19). To quantify *C. albicans* CFUs in the vagina, vaginal washes were collected for plate counting, which disclosed the most significantly

https://doi.org/10.1038/s41467-025-63110-0

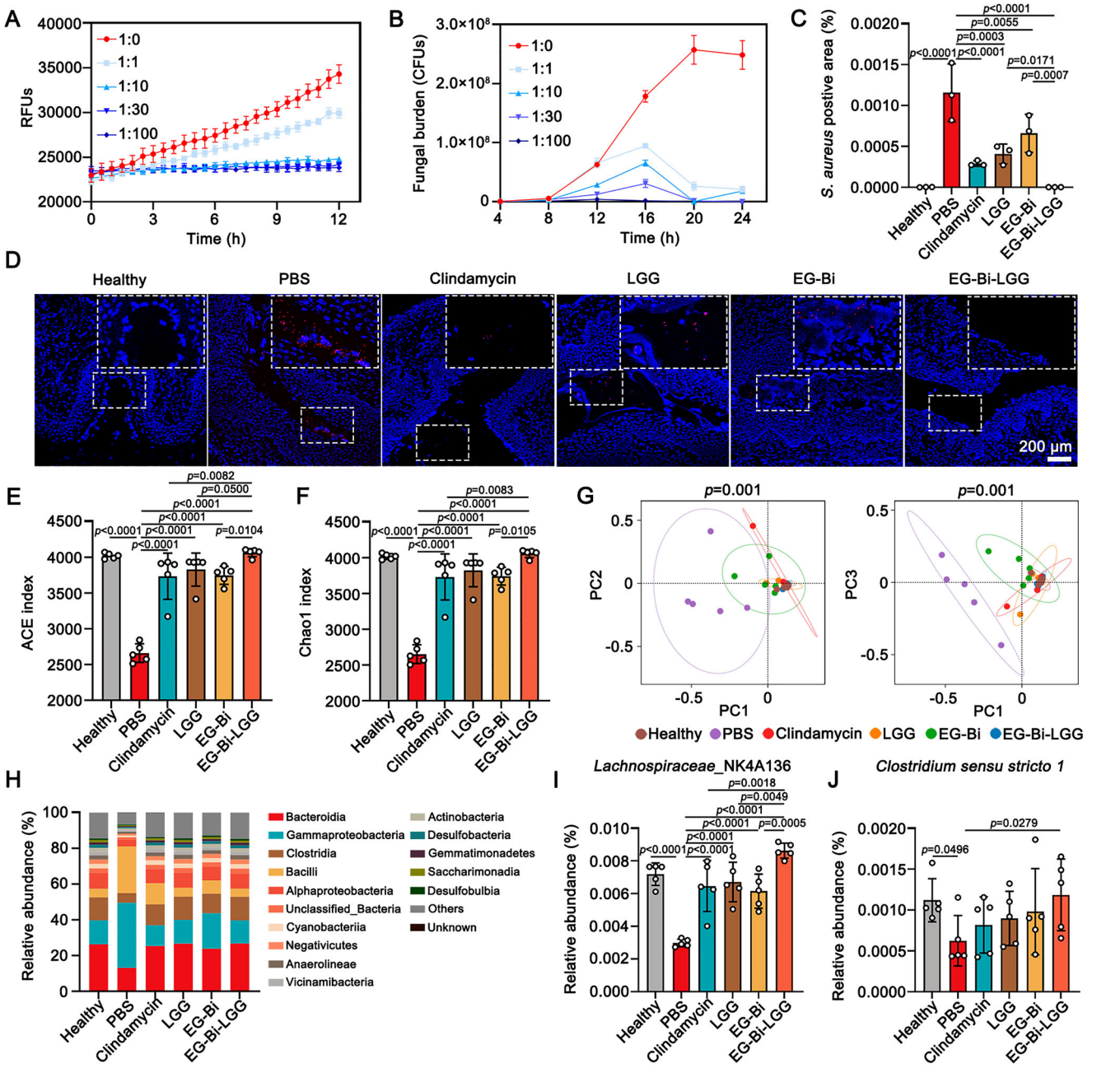

Fig. 6 | Regulation of the vaginal microbiota. In vitro competition between LGG and *S. aureus* (**A**) or *C. albicans* (**B**) at various feed ratios. *S. aureus* expressing GFP or *C. albicans* were co-incubated with LGG at 37 °C at different feed ratios of 1:0, 1:1, 1:10, 1:30, and 1:100, respectively ($n = 5$ independent samples in A; $n = 3$ independent samples in B). **C**-**J** *S. aureus*-infected mice were intravaginally administered with PBS, clindamycin, LGG, EG-Bi, or EG-Bi-LGG every day for 7 days and vaginal samples were collected for *S. aureus* detection and 16S ribosomal RNA gene sequencing. Relative area of signal in the red channel (**C**) and immunofluorescence images (**D**) of vaginal sections from treated mice ($n = 3$ independent samples). Red and blue indicate *S. aureus* expressing GFP and cell nuclei stained with DAPI, respectively. ACE index (**E**) and Chao1 index (**F**) of the vaginal microbiota ($n = 5$ independent samples). **G** Result of the PCoA of the vaginal microbiota at OTU and genus levels ($n = 5$ independent samples). **H** Relative abundances of the vaginal microbiota at the class level. Relative abundances of *Lachnospiraceae*_NK4A136 group (**I**) and *Clostridium sensu stricto 1* (**J**) in the vaginal microbiota at the genus level ($n = 5$ independent samples). Data are mean ± SD. Statistical analysis was performed using one-way ANOVA with Fisher's LSD multiple comparisons test, and *p*-values were indicated. Source data are provided as a Source Data file.

decreased fungal burden within the vagina in the clotrimazole and EG-Bi-LGG groups among all the treated groups (Fig. 8D and Supplementary Fig. 20). The levels of inflammatory cytokines were assessed and the results showed that treatments with clotrimazole and EG-Bi-LGG notably suppressed the levels of IL-1β, TNF-α, S100A7/A8, and chemoattractant KC compared to all other groups (Fig. 8E, F and Supplementary Fig. 21). Additionally, H&E staining of vaginal tissue suggested that infection-induced enhancements of vaginal keratinization and leukocyte infiltration were greatly reduced after treating with EG-Bi-LGG (Fig. 8G, H). MPO staining of the sectioned vaginal tissue further confirmed the most significant decrease of neutrophil infiltration in the EG-Bi-LGG group among all treated groups (Fig. 8I and Supplementary Fig. 22). In short, these data supported that LSTC could effectively inhibit the colonization of *C. albicans* in the vagina and ameliorate *C. albicans*-induced mucosal injury.

https://doi.org/10.1038/s41467-025-63110-0

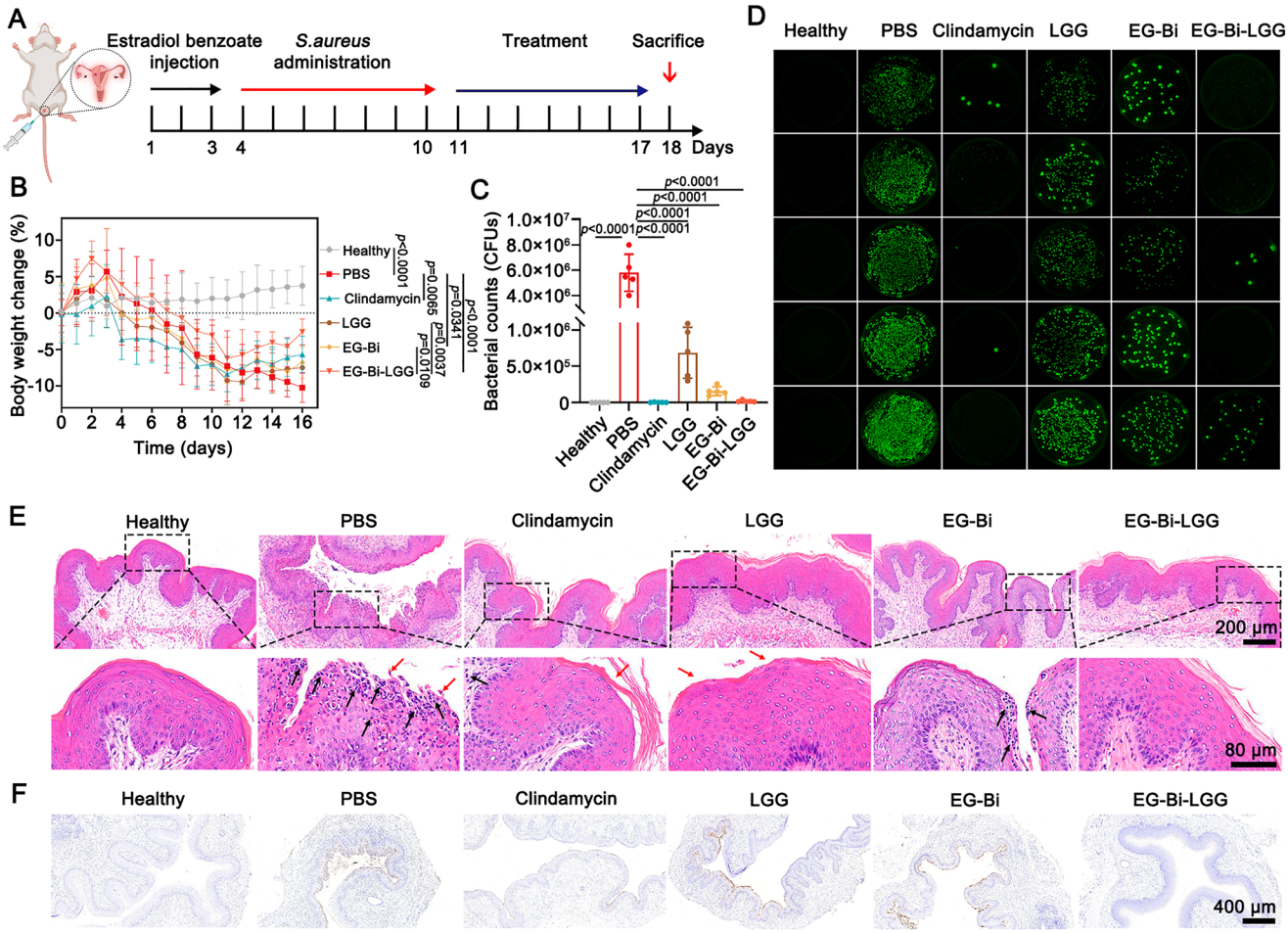

Fig. 7 | Value of LSTC in intervening aerobic vaginitis. A Experimental design of in vivo assessment using a *S. aureus*-induced murine model of aerobic vaginitis. Mice were intraperitoneally treated with 0.2 mg of estradiol benzoate every day for 3 days and subsequently were intravaginally infected with 4.0×10^9 CFUs of *S. aureus* every day for 7 days. The infected mice were then intravaginally administered with PBS, clindamycin, LGG, EG-Bi, or EG-Bi-LGG every day for 7 days. **B** Fluctuation of mouse body weight change (% of initial weight) after various treatments ($n = 5$ mice). Counts of *S. aureus* in vaginal washes on day 7 post-treatment (**C**) and corresponding fluorescence images of LB agar plates for colony counting (**D**) ($n = 5$ mice). **E** Images of H&E staining of vaginal tissues from treated mice. Black and red arrows indicate epithelial inflammation and epithelial desquamation or keratinization, respectively. **F** Images of MPO staining of vaginal tissues from treated mice. Brown indicates MPO^+ cells. Data are mean ± SD. Statistical analysis was performed using one-way ANOVA with Fisher's LSD multiple comparisons test, and *p*-values were indicated. Source data are provided as a Source Data file. The elements in Fig. 7A were created in BioRender.

In summary, we present the decoration of mucosal surfaces with LSTC to multifacetedly restore mucosal barrier functions. Under a simple yet cytocompatible condition, EG can chelate Bi^{III} ions to form a coating that can further hybridize with LGG steadily at mucosal surfaces, through metal-phenolic complexation and π-π stacking interactions. The resulting therapeutic coating is applicable to diverse bacterial species and can be generated on different types of mucosal surfaces. The combination of the barrier-repairing ability of Bi^{III} ions, the immunosuppressive feature of EG, and the microbiota-regulating behavior of LGG enables LSTC to effectively restore the physicochemical, immune, and microbial homeostasis of the mucosal barrier. Specifically, LSTC improves barrier integrity by increasing the productions of tight junctions and mucus, remits mucosal inflammation by suppressing the production of inflammatory cytokines, and maintains normal homeostasis of the microbiota by inhibiting the colonization of pathogens. During in vivo therapeutic assessment, LSTC potently alleviates vaginal pathological injury and decreases vaginal inflammatory infiltration in two murine models of aerobic vaginitis and vaginal candidiasis. Importantly, LSTC not only demonstrates comparable therapeutic efficacies to clinical antibiotics, but also outperforms in restoring microbial homeostasis, implying a low risk of antibiotic resistance and a prolonged prevention of recurrence. Note that the murine model shows significant differences in vaginal pH, microbiota composition, and hormonal regulation compared to humans, future studies on systematic assessment of biosafety, dosage regiment and treatment frequency, and batch-to-batch optimization particularly in large animal models are necessitated before considering for further translation.

Methods

Ethical Statement

ICR mice (female, 6-8 weeks old) were purchased from the SiPeiFu Biotechnology (Beijing, China) and housed in the SPF environment with an average temperature of 22 °C and a standard 12 h light/dark cycle. All animal experiments were carried out according to the institutional guidelines and approved by Animal Care and Use Committee in Shanghai Yishang Biotechnology company (IACUC-2023-Mi-214).

Materials

EG (ethyl gallate) was purchased from Shanghai Yuanye Bio-Technology (China). $Bi(NO_3)_3{\cdot}5H_2O$ (A600233) and lysogeny broth (LB, A507002) medium were obtained from Sangon Biotech (China).

https://doi.org/10.1038/s41467-025-63110-0

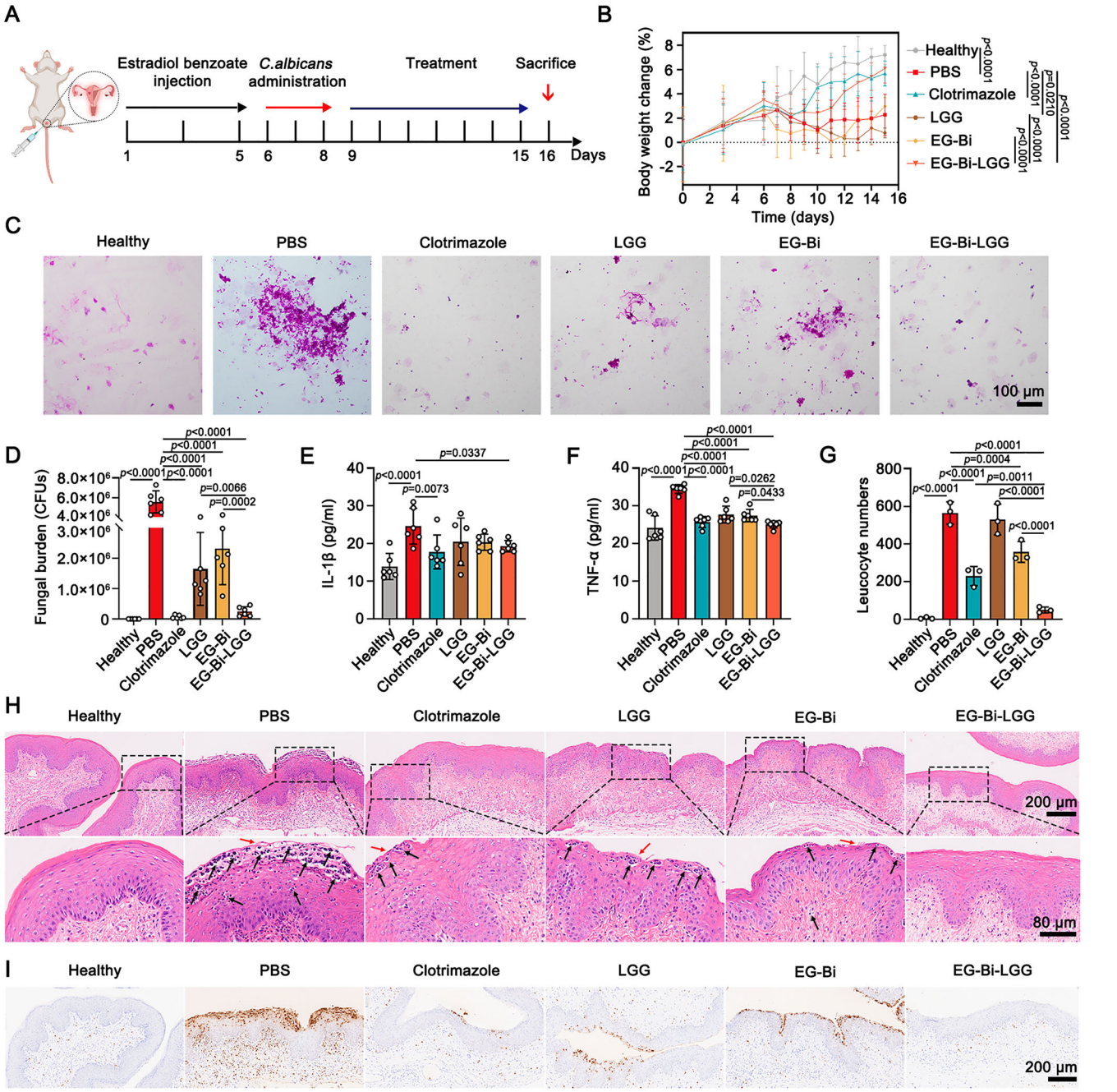

Fig. 8 | Efficacy of LSTC in treating vaginal candidiasis. A Experimental design of in vivo assessment using a *C. albicans*-induced murine model of vaginal candidiasis. Mice were intraperitoneally treated with 0.2 mg of estradiol benzoate every other day for three times and subsequently were intravaginally infected with 2.0×10^9 CFUs of *C. albicans* every day for 3 days. The infected mice were then intravaginally administered with PBS, clotrimazole, LGG, EG-Bi, or EG-Bi-LGG every day for 7 days. **B** Fluctuation of mouse body weight change (% of initial weight) after various treatments ($n = 6$ mice). **C** Images of PAS staining of vaginal secretions showing *C. albicans* ($n = 5$ mice). **D** Counts of *C. albicans* in vaginal washes on day 7 post-treatment ($n = 6$ mice). Levels of IL-1β (**E**) and TNF-α (**F**) in serum ($n = 6$ mice). **H** Images of H&E staining of vaginal tissues from treated mice. Black and red arrows indicate inflammation and epithelial desquamation or keratinization, respectively. **G** Quantification of leukocyte infiltration from (**H**) ($n = 3$ independent samples). **I** Images of MPO staining of vaginal tissues from treated mice. Brown indicates MPO^+ cells. Data are mean ± SD. Statistical analysis was performed using one-way ANOVA with Fisher's LSD multiple comparisons test, and *p*-values were indicated. Source data are provided as a Source Data file. The elements in Fig. 8A were created in BioRender.

Brain Heart Infusion Broth (BHI, HB8297), Man Rogosa Sharpe (MRS, HB0384-5), and Yeast Extract Peptone Dextrose (YPD, HB5193-1) medium were purchased from Qingdao Hope Biotechnology (China). Fetal bovine serum (FBS, 10099-141) and Dulbecco's Modified Eagle Medium (DMEM, 11965092) were purchased from Gibco. Penicillin-streptomycin (15140-122) was obtained from Hyclone. BSA-FITC (SF063), clindamycin (C9760), and clotrimazole (IC0490) were purchased from Solarbio Life Sciences (China). Cyanine 5.5 NHS ester (S276331) was purchased from Aladdin (China). FITC-dextran (FD4-100MG) and mucin (Type III, M1778) were obtained from Sigma-Aldrich. LPS (ST1470), CCK-8 Kit (C0038), H&E Staining Kit (C0105), MPO staining Kit (AF7494), AB staining Kit (C0155S), neutral balsam (C0173), Antifade Mounting Medium (P0131), and Hoechst 33342 (C1022) were obtained from Beyotime Biotechnology. Annexin V-FITC

Apoptosis Detection Kit (AP101) and IL-1β (EK201B), TNF-α (EK282), and IL-6 (EK206) ELISA kits were purchased from MultiSciences Biotech (China). Anti-occludin (sc-133256) was purchased from Santa Cruz Biotechnology, and Rabbit polyclonal antibody to ZO-1 (AF5145) was purchased from Affinity Biosciences.

Bacterial and fungal strains and cell lines

EF was obtained from the American Type Culture Collections (USA). *S. aureus* was purchased from Hangzhou Forhigh Biotech (China). EcN was purchased from Ningbo Bionice (China). LD was purchased from Shanghai Luwei Technology Co., Ltd (China). *C. albicans* was purchased from Shanghai Bioresource Collection Center (China). EF, *S. aureus*, and EcN were cultured in LB medium at 37 °C. LGG and LD were cultured in MRS medium at 37 °C. *C. albicans* was cultured on a YPD agar plate at 37 °C. Plasmids RN4220 T61-eGFP (erythromycin resistant) and pBBR1MCS2-Tac-mCherry (kanamycin resistant) were obtained from domestic suppliers and applied as received. Human vaginal epithelial cell line (VK2/E6E7) was kindly provided by Lizeng Gao (the Biophysics Chinese Academy of Sciences, Beijing, China). Mucus-producing intestinal cell line (HT29-MTX-E12) was kindly provided by Wei Wu (Fudan University, Shanghai, China). Mouse macrophage cell line (J774A.1), human epithelial-like cell line (293 T) and human colon carcinoma cell line (Caco-2) were purchased from iCell Bioscience Inc. (Shanghai, China). J774A.1, 293 T, Caco-2, VK2/E6E7, and HT29-MTX-E12 cells were cultured in DMEM medium supplemented with 10% FBS and 1% penicillin-streptomycin at 37 °C in a 5% CO_2 incubator.

In vitro preparation of EG-Bi and LSTC

To prepare the EG-Bi coating, 1 mg/ml mucin was dissolved in PBS containing 1.5% agar to form an artificial mucus layer. Then, 0.6 mg/ml EG and 0.2 mg/ml $Bi(NO_3)_3{\cdot}5H_2O$ dissolved in ddH_2O were added to the surface of the artificial mucus layer and stirred at 300 rpm for 10 min at room temperature (RT). To prepare LSTC, 5.0×10^7 CFUs/ml of LGG, 2.0×10^8 CFUs/ml of EF, LD, or EcN were further added onto the surface of the EG-Bi coating and stirred at 300 rpm for 5 min at RT.

Characterization of EG-Bi

TEM (HITACHI, Japan), SEM (HITACHI, Japan), and AFM (Bruker, USA) were used to visualize the morphologies of the EG-Bi coating. In brief, 10 μl of ddH_2O containing 0.6 mg/ml EG and 0.2 mg/ml $Bi(NO_3)_3{\cdot}5H_2O$ was dropped onto a Formvar/carbon 200-mesh grid and put for drying in the air at RT. For SEM and AFM observations, grid was replaced by silicon wafer. For CLSM (TCS SP8, Leica) observation, 0.2 mg/ml BSA-FITC was added to the surface of the resulting EG-Bi coating and stirred at 300 rpm for 10 min at RT.

Characterization of LSTC

TEM and SEM were used to visualize the morphology of LSTC. In brief, 10 μl of ddH_2O containing 0.6 mg/ml EG and 0.2 mg/ml $Bi(NO_3)_3{\cdot}5H_2O$ was dropped onto a Formvar/carbon 200-mesh grid and put for drying in the air at RT. Then, 5.0×10^7 CFUs/ml of LGG, 2.0×10^8 CFUs/ml of EF, LD, or EcN were further added onto the surface of the EG-Bi coating and the sample was dried completely in air at RT. For SEM observation, grid was replaced by the silicon wafer. Cy5.5-labeled LGG, EF, or LD and EcN expressing mCherry were used to prepare LSTC for CLSM observation. For bacterial plate counting, the resulting LSTC was homogenized and spread on MRS plates for overnight incubation at 37 °C.

In vitro cytotoxicity of EG-Bi

To assess the toxicity of EG-Bi on bacteria, LGG (1×10^5 CFUs per well, 200 μl) was resuspended in MRS medium within 96-well plate and incubated with or without the mixture of 0.6 mg/ml EG and 0.2 mg/ml $Bi(NO_3)_3{\cdot}5H_2O$ at 37 °C with gentle shaking. The absorbance at 600 nm (OD_{600}) intensity was recorded for 15 h with a 0.5-h interval by a microplate reader (BioTek, USA). To assess the cytotoxicity of EG-Bi on cells, 293 T or J774A.1 cells (1.0×10^4 per well, 100 μl) were seeded into a 96-well plate and cultured overnight at 37 °C. Then, a mixture of 0.6 mg/ml EG and 0.2 mg/ml $Bi(NO_3)_3{\cdot}5H_2O$ was added to the plate and incubated at 37 °C for 6, 12, and 24 h, respectively. Resultant cells were further incubated with CCK-8 solution for 3 h at 37 °C, and the absorbance was measured at 450 nm by a microplate reader.

Ex vivo preparation of LSTC

To prepare LSTC on ex vivo colon tissue, the freshly sampled colon tissue from ICR mice (female, 6-8 weeks old) was everted to expose the mucosal surface. Then, the colon tissue was divided into ~1.5 cm segments, and the two ends of the everted colon were carefully ligated. The prepared colon segments were immersed in a ddH_2O solution containing 0.6 mg/ml EG and 0.2 mg/ml $Bi(NO_3)_3{\cdot}5H_2O$ and shaken at 300 rpm for 10 min. After washing with PBS for three times, 500 μl of 5×10^7 CFUs/ml Cy5.5-labeled LGG were incubated with colon segments decorated with or without EG-Bi at 300 rpm for 5 min. To prepare LSTC on ex vivo vaginal tissue, the freshly sampled vaginal tissue from ICR mice (female, 6-8 weeks old) was sectioned longitudinal and immobilized on a 6-well plate to ensure an upward orientation of the mucosal layer. Then, a 500 μl of ddH_2O solution containing 0.6 mg/ml EG and 0.2 mg/ml $Bi(NO_3)_3{\cdot}5H_2O$ was added on the surface of the mucosal layer and shaken at 300 rpm for 10 min. After washing with PBS for three times, 500 μl of 5×10^7 CFUs/ml Cy5.5-labeled LGG was incubated with vaginal tissue decorated with or without EG-Bi at 300 rpm for 20 min. After washing with PBS for three times, the resultant colon segments or vaginal tissues were imaged using IVIS. To quantify the hybridized bacteria, homogenates of the colon segments or vaginal tissues were spread onto MRS plates for overnight incubation at 37 °C. To quantify the content of Bi^{III} ions in the coating, homogenates of the colon segments were centrifuged and the supernatant was detected by ICP-MS.

In vivo preparation of LSTC

ICR mice (female, 6-8 weeks old) were administered by rectal or vaginal injection of PBS (50 μl) containing 0.6 mg/ml EG and 0.2 mg/ml $Bi(NO_3)_3{\cdot}5H_2O$, followed by PBS (20 μl) containing 5×10^7 CFUs/ml Cy5.5-labeled LGG. Mice injected with equivalent Cy5.5-labeled LGG were used as a control. At 6 h post injection, mice were anesthetized and imaged using IVIS. Then, mice were euthanized and the colonic or vaginal tissues were harvested for IVIS imaging. The images of the mice and tissues were recorded and analyzed by Living Image 4.2. In addition, equivalent samples were grinded and diluted with 1 ml of PBS. The dilutions (50 μl) from both tissues were spread onto MRS agar plate for an overnight incubation at 37 °C.

In vivo stability of LSTC

After in vivo formation of LSTC in the vaginal tract, ICR mice (female, 6-8 weeks old) were anesthetized, and the fluorescence signal of the mice at the Cy5.5 channel was monitored using IVIS at a 6-h interval for 2 days. Then, the mice were euthanized, and vaginal tissues were harvested at 0, 6, 12, 18, or 24 h after administration. The tissues were homogenized for quantifying the amount of Bi^{III} ions and the counts of LGG, respectively.

In vitro microbial competition

To assess the competition between LGG and *S. aureus*, LGG and *S. aureus* (erythromycin resistance, expressing GFP) were separately grown in MRS and LB medium at 37 °C for 12 h and subsequently diluted to a concentration of 1×10^7 CFUs/ml. *S. aureus* and LGG were then mixed in BHI medium (pH 6.0) in a series of ratios (1:1, 1:10, 1:30, 1:100) and 100 μl of each mixture was incubated at 37 °C with shaking. The relative fluorescence units (RFUs) of GFP expressed by *S. aureus* were recorded at 490/530 nm at a 0.5-h interval. To assess the

competition between LGG and *C. albicans*, LGG and *C. albicans* were separately grown in MRS and YPD medium at 37 °C for 12 h and subsequently diluted to a concentration of 1×10^7 CFUs/ml. *C. albicans* and LGG were mixed in medium (MRS:YPD = 1:1) in a series of ratios (1:1, 1:10, 1:30, 1:100) and incubated at 37 °C with shaking. Then, 50 μl of each sample was diluted and spread onto YPD agar plates at determined time points and incubated at 37 °C overnight for bacterial counting. To assess the adhesion and growth of *S. aureus* and *C. albicans* at LSTC decorated on an artificial mucus layer, 3×10^5 CFUs of *S. aureus* or *C. albicans* were further added onto the surface of LSTC, followed by stirring at 300 rpm for 5 min at RT. After incubation at 37 °C for various time points, the intact artificial mucus was collected and homogenized for bacterial plate counting.

In vitro anti-inflammatory effect of EG

J774A.1 cells (1.0×10^5 per well, 500 μl) were seeded into a 48-well plate and cultured overnight at 37 °C. Then, LPS (1 μg/ml) and different concentrations of EG (1.25, 2.5, 5, and 10 μg/ml) were added to the plate and incubated at 37 °C. The cell supernatants were collected at 4, 8, and 12 h for separately detecting the levels of TNF-α, IL-6, and IL-1β. These cytokines were detected using ELISA assay following the manufacturer's instructions. The results were determined at 450 nm wavelength within 30 min by a microplate reader. VK2 cells (2.0×10^5 per well, 1 ml) were seeded into a 6-well plate and cultured overnight at 37 °C. Then, 50 μg/ml LPS and 10 μg/ml EG were added to the plate and incubated at 37 °C for 24 h. Subsequently, the resultant cells were harvested and washed twice with precooled PBS. Then, apoptosis level of VK2 cells was assessed by Annexin V-FITC Apoptosis Detection Kit according to the manufacturer's protocol. The result was detected using FACSVerse flow cytometer (BD Biosciences, USA), and data analysis was performed using FlowJo (TreeStar).

Permeability and TEER measurements

To form an epithelial cell monolayer, 5×10^4 of VK2 cells were seeded into a 24-well transwell insert (Corning, 0.4 μm pore size) and cultured for 4 days with a 2-day interval of medium replacement. Then, 3 μg/ml $Bi(NO_3)_3{\cdot}5H_2O$ was added to the apical insert in the presence of 50 μg/ml LPS and co-incubated for 24 h. For permeability measurement, 1 mg/ml FITC-dextran (4 kDa) was added to the apical insert and co-incubated for 4 or 24 h. The medium in basolateral side was collected and diluted with PBS. The concentration of FITC-dextran was detected at 490/530 nm by a microplate fluorometer (Infinite M200 PRO, Tecan). For TEER measurement, one electrode was placed in the apical insert, while a second electrode was placed in the basolateral side. TEER values were measured using a Millicell-ERS volt-ohmmeter (EVOM, World Precision Instruments, USA) to monitor the electrical resistance. TEER values were calculated using the following formula:

$$\mathrm{TEER} = R \times A$$

where R is the electrical resistance of the barrier with monolayer and A is the apical insert area.

In vitro physicochemical barrier function

VK2 cells (5.0×10^5) were seeded into glass-bottom dishes and cultured overnight at 37 °C. Then, cells were stimulated with 50 μg/ml LPS and concurrently incubated with 3 μg/ml $Bi(NO_3)_3{\cdot}5H_2O$ at 37 °C for 24 h. After washing with PBS, VK2 cells were fixed with 4% paraformaldehyde (PFA) for 20 min and subsequently blocked with 5% BSA for 30 min. Then, resultant VK2 cells were stained with anti-mouse occludin (1:50) and ZO-1 (1:100) at 4 °C overnight, followed by corresponding secondary antibodies for 1 h at RT. After washing with PBS, these cells were incubated with 1 μg/ml Hoechst 33342 for 20 min at RT. The fluorescence intensity was observed and captured by CLSM. To assess the mucus, VK2 cells were processed AB staining in accordance with the manufacturer's instructions.

Efficacy of LSTC in treating aerobic vaginitis and vaginal candidiasis

To establish the murine model of aerobic vaginitis, ICR mice (female, 6-8 weeks old) were subcutaneously injected with 0.1 ml of 2 mg/ml estradiol benzoate every day for 3 days. Subsequently, mice were intravaginally administered with 10 μl of 4.0×10^9 CFUs/ml *S. aureus* every day for 7 days. Then, the mice were randomly divided to five groups and intravaginally treated with PBS, clindamycin (6.5 mg/kg), EG-Bi (12 μg of EG and 4 μg of $Bi(NO_3)_3{\cdot}5H_2O$), LGG (5×10^7 CFUs), EG-Bi-LGG (12 μg of EG, 4 μg of $Bi(NO_3)_3{\cdot}5H_2O$, and 5×10^7 CFUs of LGG) every day for 7 days. To induce the murine model of vaginal candidiasis, ICR mice (female, 6-8 weeks old) were subcutaneously injected with 0.1 ml of 2 mg/ml estradiol benzoate every other day for three times. Subsequently, mice were intravaginally administered with 10 μl of 2.0×10^9 CFUs/ml *C. albicans* every day for 3 days. Then, the mice were randomly divided to five groups and intravaginally treated with PBS, clotrimazole (0.4 mg/kg), EG-Bi (12 μg of EG and 4 μg of $Bi(NO_3)_3{\cdot}5H_2O$), LGG (5×10^7 CFUs), EG-Bi-LGG (12 μg of EG, 4 μg of $Bi(NO_3)_3{\cdot}5H_2O$, and 5×10^7 CFUs of LGG) every day for 7 days. Healthy mice without infection were used as a control in both above models. The body weight of mice was monitored every day. At the endpoint of the experiment, vaginal washes were collected for the assessment of *S. aureus* or *C. albicans* counts. Serum was collected for detecting the levels of inflammatory cytokines using the ELISA kit, and vaginal tissue was sampled for pathological analysis using H&E staining.

Microbiota 16S ribosomal RNA gene sequencing and analysis

In brief, bacterial DNA was extracted from vaginal washes of *S. aureus*-infected female ICR mice after various treatments. Sequencing was performed by targeting hypervariable V3-V4 regions of the bacterial 16S ribosomal RNA gene with universal primers 27F-1492R (27 F: AGRGTTTGATYNTGGCTCAG; 1492 R: TASGGHTACCTTGTTASGACTT) and detected on the Illumina HiSeq platform. The class or genus classification was obtained on the basis of the sequence composition of the OTU. The alpha diversity was analyzed with ACE and Shannon index to examine the richness and diversity of species in individual samples, while beta diversity was analyzed with PCoA to evaluate the similarity in bacterial composition. Data analysis was performed on BMKCloud.

Transcriptome sequencing and pathway analysis

Briefly, total RNA was extracted from the vaginal tissue of *S. aureus*-infected female ICR mice after various treatments using TRIzol® Reagent in accordance with manufacturer's protocol. The RNA quality, in terms of 260/280 and 260/230 ratios, was measured by 5300 Bioanalyser (Agilent Technologies), and its quantity was determined using NanoDrop (ND-2000, Thermo Fisher Scientific). Then, RNA purification, reverse transcription, library construction, and sequencing were performed at Shanghai Majorbio Bio-pharm Biotechnology Co., Ltd. (Shanghai, China) in accordance with the manufacturer's instructions (Illumina, San Diego, CA). To identify DEGs between two different samples, the expression level of each transcript was calculated in accordance with the transcripts per million (TPM) method. RNA-Seq by Expectation-Maximization (RSEM) was applied for quantifying transcript abundances, and DEGs were identified using DESeq2. Genes with $|\log_2(\text{fold change})| \geq 1$ and false discovery rate (FDR) ≤ 0.05 were considered as DEGs. GO functional enrichment and KEGG pathway analysis of DEGs were performed using Goatools and KOBAS, respectively. GSEA was performed using the R package clusterProfiler (version 4.10.0). The fold changes of genes between case and control

group calculated previously were used to generate the gene list in a descending order.

Immunohistochemical and immunofluorescence analysis

The collected vaginal tissue was fixed in 4% PFA and then embedded in paraffin. Then, the sample was cut into 4-μm sections. After deparaffinization and antigen retrieval, the obtained sections were blocked with 10% goat serum for 1 h. Subsequently, the sections were incubated with primary antibodies, including occludin (1:200) or ZO-1 (1:200) at 4 °C overnight, followed by corresponding secondary antibodies conjugated with fluorescence or HRP for 1 h at RT. To examine mucus, the sections were incubated with AF488-WGA (1:100) at 37 °C for 30 min. For immunohistochemical analysis, samples were covered by neutral balsam and observed under an upright microscope (Nikon, Japan). For immunofluorescence analysis, samples were covered by Antifade Mounting Medium with DAPI and captured by CLSM. ImageJ software (Media Cybernetics, USA) was used to analyze the positive signal in the section.

Statistical analysis

All of the data are presented as mean ± SD. The statistical differences between the two groups were compared using the unpaired Student's *t*-test. One-way ANOVA or two-way ANOVA with Fisher's LSD post-test was used to compare multiple comparisons. Statistical analyses were conducted using GraphPad Prism 8.0. In all cases, statistical significance was accepted at $p < 0.05$.

Reporting summary

Further information on research design is available in the Nature Portfolio Reporting Summary linked to this article.

Data availability

All sequencing data generated in this study have been deposited in the China National Center for Bioinformation [https://www.cncb.ac.cn]. The 16S ribosomal RNA gene-sequencing data are deposited under accession GSA number CRA021925. The RNA sequencing data are deposited under GSA number CRA021846. The remaining data are available within the Article, Supplementary Information, or Source data for the figures provided with this paper. Source data are provided with this paper.

References

1. Johansson, M. E. V. et al. The inner of the two Muc2 mucin-dependent mucus layers in colon is devoid of bacteria. *Proc. Natl. Acad. Sci. USA* **105**, 15064–15069 (2008).
2. Chen, Y. et al. Reinforcement of the intestinal mucosal barrier via mucus-penetrating PEGylated bacteria. *Nat. Biomed. Eng.* **8**, 823–841 (2024).
3. Cai, R. et al. Interactions of commensal and pathogenic microorganisms with the mucus layer in the colon. *Gut Microbes*. **11**, 680–690 (2020).
4. Kundu, P., Blacher, E., Elinav, E. & Pettersson, S. Our gut microbiome: the evolving inner self. *Cell* **171**, 1481–1493 (2017).
5. Peterson, L. W. Intestinal epithelial cells: regulators of barrier function and immune homeostasis. *Nat. Rev. Immunol.* **14**, 141–153 (2014).
6. Swindle, E. J., Collins, J. E. & Davies, D. E. Breakdown in epithelial barrier function in patients with asthma: identification of novel therapeutic approaches. *J. Allergy Clin. Immunol.* **124**, 23–34 (2009).
7. Turner, J. R. Intestinal mucosal barrier function in health and disease. *Nat. Rev. Immunol.* **9**, 799–809 (2009).
8. Mills, R. H. et al. Multi-omics analyses of the ulcerative colitis gut microbiome link bacteroides vulgatus proteases with disease severity. *Nat. Microbiol.* **7**, 262–276 (2022).
9. Colombel, J.-F. et al. Adalimumab induces deep remission in patients with Crohn's disease. *Clin. Gastroenterol. Hepatol.* **12**, 414–422 (2014).
10. Colombel, J. F. et al. Infliximab, azathioprine, or combination therapy for Crohn's disease. *N. Engl. J. Med.* **362**, 1383–1395 (2010).
11. Chapman, T. P. & Satsangi, J. Head-to-head biologic therapy in Crohn's disease. *Lancet*. **399**, 2169–2171 (2022).
12. Cunningham, K. E. & Turner, J. R. Myosin light chain kinase: pulling the strings of epithelial tight junction function. *Ann. N. Y Acad. Sci.* **1258**, 34–42 (2012).
13. Jin, Y. & Blikslager, A. T. The regulation of intestinal mucosal barrier by myosin light chain kinase/rho kinases. *Int J. Mol. Sci.* **21**, 3550 (2020).
14. Bakshani, C. R. et al. Evolutionary conservation of the antimicrobial function of mucus: a first defence against infection. *Npj Biofilms Microbiomes* **4**, 1–12 (2018).
15. Barr, J. J. et al. Bacteriophage adhering to mucus provide a non-host-derived immunity. *Proc. Natl. Acad. Sci. USA* **110**, 10771–10776 (2013).
16. Metidji, A. et al. The environmental sensor AHR protects from inflammatory damage by maintaining intestinal stem cell homeostasis and barrier integrity. *Immunity* **49**, 353–362.e5 (2018).
17. Kim, S. et al. Mucin degrader Akkermansia muciniphila accelerates intestinal stem cell-mediated epithelial development. *Gut Microbes* **13**, 1–20 (2021).
18. Haderer, M. et al. Novel pathomechanism for spontaneous bacterial peritonitis: disruption of cell junctions by cellular and bacterial proteases. *Gut*. **71**, 580–592 (2022).
19. Thaiss, C. A., Zmora, N., Levy, M. & Elinav, E. The microbiome and innate immunity. *Nature* **535**, 65–74 (2016).
20. Honda, K. & Littman, D. R. The microbiota in adaptive immune homeostasis and disease. *Nature* **535**, 75–84 (2016).
21. Kwak, S. Y. et al. Metallothionein 2 activation by pravastatin reinforces epithelial integrity and ameliorates radiation-induced enteropathy. *EBioMedicine* **73**, 103641 (2021).
22. Schneditz, G. et al. Enterotoxicity of a nonribosomal peptide causes antibiotic-associated colitis. *Proc. Natl. Acad. Sci. USA* **111**, 13181–13186 (2014).
23. Zeng, M. Y., Inohara, N. & Nuñez, G. Mechanisms of inflammation-driven bacterial dysbiosis in the gut. *Mucosal. Immunol.* **10**, 18–26 (2017).
24. Pruski, P. et al. Assessment of microbiota: host interactions at the vaginal mucosa interface. *Methods* **149**, 74–84 (2018).
25. Denning, D. W., Kneale, M., Sobel, J. D. & Rautemaa-Richardson, R. Global burden of recurrent vulvovaginal candidiasis: a systematic review. *Lancet Infect. Dis.* **18**, 339–347 (2018).
26. Fan, C. et al. Aerobic vaginitis induced by Escherichia coli infection during pregnancy can result in adverse pregnancy outcomes through the IL-4/JAK-1/STAT-6 pathway. *Front. Microbiol* **12**, 651426 (2021).
27. Oh, K. Y. et al. Composition of vaginal microbiota in pregnant women with aerobic vaginitis. *Front Cell Infect. Microbiol*. **11**, 677648 (2021).
28. Schwebke, J. R., Muzny, C. A. & Josey, W. E. Role of gardnerella vaginalis in the pathogenesis of bacterial vaginosis: a conceptual model. *J. Infect. Dis.* **210**, 338–343 (2014).
29. Berman, J. & Sudbery, P. E. *Candida Albicans*: a molecular revolution built on lessons from budding yeast. *Nat. Rev. Genet*. **3**, 918–930 (2002).
30. Fang, L. et al. Metastable iron sulfides gram-dependently counteract resistant Gardnerella vaginalis for bacterial vaginosis treatment. *Adv. Sci.* **9**, 2104341 (2022).
31. Luo, H. et al. Encoding bacterial colonization and therapeutic modality by wrapping with an adhesive drug-loadable nanocoating. *Mater. Today* **62**, 98–110 (2023).

32. Alonso-Roman, R. et al. *Lactobacillus rhamnosus* colonisation antagonizes *Candida albicans* by forcing metabolic adaptations that compromise pathogenicity. *Nat. Commun.* **13**, 3192 (2022).
33. Si, W. et al. *Lactobacillus rhamnosus* GG induces cGAS/STING-dependent type I interferon and improves response to immune checkpoint blockade. *Gut*. **71**, 521–533 (2021).
34. France, M., Alizadeh, M., Brown, S., Ma, B. & Ravel, J. Towards a deeper understanding of the vaginal microbiota. *Nat. Microbiol* **7**, 367–378 (2022).
35. Zhang, X. et al. Hollow microcapsules with ulcerative colitis therapeutic effects made of multifunctional Turkish galls extraction. *ACS Appl. Mater. Interfaces* **11**, 25054–25065 (2019).
36. Yu, W. et al. Photoaffinity labelling-based chemoproteomic strategy identifies PEBP1 as the target of ethyl gallate against macrophage activation. *Chem. Commun.* **59**, 1022–1025 (2023).
37. Wang, Q. et al. All-in-one theranostic platform based on hollow microcapsules for intragastric-targeting antiulcer drug delivery, CT imaging, and synergistically healing gastric ulcer. *Small* **18**, 2104660 (2022).
38. Li, H., Wang, R. & Sun, H. Systems approaches for unveiling the mechanism of action of bismuth drugs: new medicinal applications beyond helicobacter pylori infection. *Acc. Chem. Res.* **52**, 216–227 (2019).
39. Guo, Y., Sun, Q., Wu, F.-G., Dai, Y. & Chen, X. Polyphenol-containing nanoparticles: synthesis, properties, and therapeutic delivery. *Adv. Mater.* **33**, e2007356 (2021).
40. Johansson, M. E. V., Larsson, J. M. H. & Hansson, G. C. The two mucus layers of colon are organized by the MUC2 mucin, whereas the outer layer is a legislator of host-microbial interactions. *Proc. Natl. Acad. Sci. USA* **108**, 4659–4665 (2011).
41. Godha, K., Tucker, K. M., Biehl, C., Archer, D. F. & Mirkin, S. Human vaginal pH and microbiota: an update. *Gynecol. Endocrinol.* **34**, 451–455 (2018).
42. Kaiko, G. E. & Stappenbeck, T. S. Host-microbe interactions shaping the gastrointestinal environment. *Trends Immunol.* **35**, 538–548 (2014).
43. Kuo, W.-T. et al. The tight junction protein ZO-1 is dispensable for barrier function but critical for effective mucosal repair. *Gastroenterology* **161**, 1924–1939 (2021).
44. Feldman, G. J., Mullin, J. M. & Ryan, M. P. Occludin: structure, function and regulation. *Adv. Drug Deliv. Rev.* **57**, 883–917 (2005).
45. Yang, N. & Sun, H. Biocoordination chemistry of bismuth: recent advances. *Coord. Chem. Rev.* **251**, 2354–2366 (2007).
46. Pelaseyed, T. et al. The mucus and mucins of the goblet cells and enterocytes provide the first defense line of the gastrointestinal tract and interact with the immune system. *Immunol. Rev.* **260**, 8–20 (2014).
47. Paone, P. & Cani, P. D. Mucus barrier, mucins and gut microbiota: the expected slimy partners?. *Gut* **69**, 2232–2243 (2020).
48. Nazari, H. et al. Advances in TEER measurements of biological barriers in microphysiological systems. *Biosens. Bioelectron.* **234**, 115355 (2023).
49. Zhang, Q. et al. A multifunctional nanotherapy for targeted treatment of colon cancer by simultaneously regulating tumor microenvironment. *Theranostics* **9**, 3732–3753 (2019).
50. Xiao, B. et al. Orally targeted delivery of tripeptide KPV via hyaluronic acid-functionalized nanoparticles efficiently alleviates ulcerative colitis. *Mol. Ther.* **25**, 1628–1640 (2017).
51. Zang, J. et al. Screening for active constituents in Turkish galls against ulcerative colitis by mass spectrometry guided preparative chromatography strategy: in silico, in vitro and in vivo study. *Food Funct.* **9**, 5124–5138 (2018).
52. Yáñez, A. et al. Granulocyte-monocyte progenitors and monocyte-dendritic cell progenitors independently produce functionally distinct monocytes. *Immunity* **47**, 890–902 (2017).
53. Zhang, Y. S. et al. Acetylation licenses Th1 cell polarization to constrain Listeria monocytogenes infection. *Cell Death Differ.* **29**, 2303–2315 (2022).
54. Koh, C.-H., Lee, S., Kwak, M., Kim, B.-S. & Chung, Y. CD8 T-cell subsets: heterogeneity, functions, and therapeutic potential. *Exp. Mol. Med.* **55**, 2287–2299 (2023).
55. Hillier, S. L., Krohn, M. A., Rabe, L. K., Klebanoff, S. J. & Eschenbach, D. A. The normal vaginal flora, H_2O_2-producing lactobacilli, and bacterial vaginosis in pregnant women. *Clin. Infect. Dis.* **16**, S273–S281 (1993).
56. Palmeira-de-Oliveira, R., Palmeira-de-Oliveira, A. & Martinez-de-Oliveira, J. New strategies for local treatment of vaginal infections. *Adv. Drug Deliv. Rev.* **92**, 105–122 (2015).
57. Gui, Y. et al. Bioinspired gelated cell sheet-supported lactobacillus biofilm for aerobic vaginitis diagnosis and treatment. *Sci. Adv.* **10**, eadq2732 (2024).
58. K, T.-W., F, W. & P, N. Incidence and symptom profiling of vaginitis containing aerobic and anaerobic pathogens. *Am. J. Obstet. Gynecol.* **230**, S641–S642 (2024).
59. Tempera, G., Bonfiglio, G., Cammarata, E., Corsello, S. & Cianci, A. Microbiological/clinical characteristics and validation of topical therapy with kanamycin in aerobic vaginitis: a pilot study. *Int J. Antimicrob. Agents* **24**, 85–88 (2004).
60. Wei, G. et al. A probiotic nanozyme hydrogel regulates vaginal microenvironment for candida vaginitis therapy. *Sci. Adv.* **9**, eadg0949 (2023).
61. Lee, Y., Puumala, E., Robbins, N. & Cowen, L. E. Antifungal drug resistance: molecular mechanisms in *candida albicans* and beyond. *Chem. Rev.* **121**, 3390–3411 (2021).

Acknowledgements

This work was financially supported by the National Key Research and Development Program of China (2021YFA0909400 to J.L.) and the National Natural Science Foundation of China (22425505 to J.L., 82360830 to W.Y., 32301099 to L.W., 32201144 to S.L., 82204503 to H.L., 52273209 to X.J.).

Author contributions

J.L., L.W. and X.J. conceived and designed the experiments with W.Y. W.Y., H.L., B.H., S.L., Q.L., R.X. and H.T. performed all experiments. All authors analysed and discussed the data. W.Y., L.W., and J.L. wrote the paper.

Competing interests

The authors declare no competing interests.

Additional information

Supplementary information The online version contains supplementary material available at https://doi.org/10.1038/s41467-025-63110-0.

Correspondence and requests for materials should be addressed to Xin Jia, Lu Wang or Jinyao Liu.

Peer review information *Nature Communications* thanks Chao Li, Lei Zhang, Barbara Giordani, and the other, anonymous, reviewer for their contribution to the peer review of this work. A peer review file is available.